R-10-51

Titanium alloys as alternative material for the supercontainer shell in the KBS-3H concept

A preliminary Ti-clay interaction study

Paul Wersin, Gruner Ltd

Daniel Grolimund, Paul Scherrer Institute

Sirpa Kumpulainen, Leena Kiviranta
B+ Tech Oy

Jocelyne Brendlé, University of Mulhouse

Margit Snellman, Saanio & Riekkola Oy

December 2010

Svensk Kärnbränslehantering AB
Swedish Nuclear Fuel
and Waste Management Co

Box 250, SE-101 24 Stockholm
Phone +46 8 459 84 00

ISSN 1402-3091
SKB R-10-51

Titanium alloys as alternative material for the supercontainer shell in the KBS-3H concept

A preliminary Ti-clay interaction study

Paul Wersin, Gruner Ltd

Daniel Grolimund, Paul Scherrer Institute

Sirpa Kumpulainen, Leena Kiviranta
B+ Tech Oy

Jocelyne Brendlé, University of Mulhouse

Margit Snellman, Saanio & Riekkola Oy

December 2010

Keywords: KBS-3H, Supercontainer shell, Titanium, Ti-clay interactions

Abstract

Ti alloys have been proposed as alternative materials to steel for the supercontainer shell surrounding the bentonite buffer in the KBS-3H disposal concept. Ti-based materials display high strength and are known to behave chemically inert under a variety of conditions. This preliminary study addresses the suitability of titanium as supercontainer material with regard to the performance of the clay buffer. Thus, possible titanium-bentonite interactions which may adversely affect the buffer's safety functions are evaluated by means of a literature and a preliminary experimental assessment.

Titanium metals display very low corrosion rates (< 1 nm/a) over a large range of pH and Eh conditions. The corrosion behaviour is governed by the low solubility of tetravalent TiO_2 which forms a passive surface corrosion layer under both oxic and reducing conditions. The interactions between titanium and clay have been barely studied so far. Preliminary long-term data obtained by Prof. Olefjord and co-workers from Chalmers (S) in the 1980ies (as part of SKB's canister program) suggests similar corrosion rates in compacted bentonite compared to those measured in water, i.e. <1 nm/a. So far, no work on reaction products from this interaction process has been carried out. Even the speciation of Ti in natural clays is uncertain. In principle, four possible reaction products resulting from Ti-clay interactions are possible: (i) Ti sorbed to the clay surface via cation exchange or specific adsorption, (ii) Ti incorporated in the octahedral or tetrahedral clay structure, (iii) Ti precipitated as separate TiO_2 or mixed (Fe, Ti) oxide, (iv) Ti precipitated as separate silicate phase and (v) polymerized as cross-linked TiO_2 units in the interlayer (Ti pillared clay). The latter two transformation products would have the strongest impact on the buffer, but are improbable on the basis of current knowledge.

A preliminary batch-type investigation has been carried out to shed more light on Ti-clay interaction processes and on the Ti species resulting from these interactions. Purified MX-80 bentonite was mixed with metallic Ti nanopowder and foil at different pH and temperature conditions. After several months, solid and solute samples from the first set of tests were analyzed by wet chemistry and quantitative X-ray fluorescence analysis. The chemical speciation of Ti was analyzed with XAS. In addition to reacted samples, a number of reference and starting materials (e.g. MX-80, Rokle bentonite, Opalinus Clay, Illite du Puy) were characterized by XRF and XAS. Preliminary results can be summarized as:

- Natural clay materials contain significant but variable amounts of Ti. The standard purification procedure for bentonites to remove accessories does not or only barely remove Ti.
- The Ti in the natural clay materials Rokle bentonite, Opalinus Clay and Illite du Puy occurs as microcrystalline TiO_2 (presumably as anatase). On the other hand, the Ti spectra in MX-80 suggest the presence of structural Ti in the smectite, but the evidence is not conclusive so far.
- The exposure of purified MX-80 to titanium powder at room temperature within a period of five months did not lead to measurable additional Ti in the clay.

A second series of experiments with synthetic "Ti-free" montmorillonite at higher temperatures (80°C) was conducted for a period of 4.5 months in order to increase Ti transfer rates from the metal surfaces to the clay. As revealed from spectroscopic analysis (micro-XRF and XANES) on the reacted materials, the use of synthetic montmorillonite combined with the increase of temperature allowed to partly overcome the experimental problems noted in the first series. Thus, Ti background concentrations were effectively very low and Ti transfer to the clay could be identified with spectroscopic analysis. On the other hand, the spectroscopic data highlighted further weaknesses in the setup. Thus the use of Ti nanopowder is not recommendable because of difficult separation from the clay.

It is recommended to carry out a third experimental series of "accelerated tests" with an optimized experimental setup.

Keywords: KBS-3H, supercontainer shell, titanium, Ti-clay interactions

Contents

1 Introduction

The KBS-3 method, based on multiple barriers, is the selected spent fuel disposal method in both Sweden and Finland. There are two design alternatives for the KBS-3 method: KBS-3V in which the canisters are emplaced in individual vertical deposition holes and KBS-3H in which several canisters are emplaced in horizontal deposition drifts. Posiva and SKB are conducting a joint research, demonstration and development (RD&D) programme with the overall aim of establishing whether KBS-3H represents a feasible alternative to the reference alternative KBS-3V. The central component in the KBS-3H disposal concept is the supercontainer shell (SC) surrounding the canister and the bentonite blocks (Figure 1-1). In the present design, the SC is composed of perforated carbon steel with a thickness of 8 mm. As has been pointed out previously (e.g. Johnson et al. 2005), steel corrosion may induce adverse effects, such as elevated H_2 pressures and alteration of the swelling bentonite. Also, large amounts of Fe corrosion products will be generated. Based on current knowledge, these effects are expected to have a limited impact, but uncertainties remain, in particular with regard to effects of Fe-bentonite interaction on smectite stability (Wersin et al. 2008).

In view of the potentially adverse effects resulting from carbon steel corrosion and the difficulty to describing these in detail, alternative materials for the SC, such as stainless steel, Ni- and Ti-based alloys have been proposed. From a first evaluation, King (2007) recommended to consider titanium alloy (Ti Grade 2) as alternative material in view of its high strength and inert geochemical behaviour in spite of its higher cost relative to the other materials.

One of the drawbacks of Ti for usage in the EBS is its poorly known physico-chemical behaviour in this environment and very few relevant studies along these lines exist. Thus, the further consideration of Ti as alternative requires the setup of a research program. In particular, the long-term behaviour of Ti in a bentonitic environment and its interaction with the clay materials should be assessed. Unfortunately, the benign inert behaviour of Ti makes it difficult to perform meaningful experiments. Hence it is not surprising that so far, very little research work on this topic has been carried out and experience is very limited.

Notwithstanding the experimental difficulties, the appropriateness of Ti alloy as SC material needs to be demonstrated. The primary focus for R&D within the KBS-3H programme should be on the possible long-term impact of Ti on the safety functions of the buffer. Thus, it needs to be demonstrated that the use of Ti in the EBS will not induce detrimental effects. Furthermore, at a more general level, it is necessary to acquire basic knowledge on Ti-clay interaction phenomena in an EBS environment.

The Ti-clay interaction programme is still in an initial stage. First a literature study including a feasibility evaluation for experimental work was performed. Based on this study, a series of batch-type pre-tests was started, some of which have been analyzed after several months of reaction time. In this report, the results from the first series of pre-tests are presented (Chapter 4). Based on the results from these pre-tests, a plan for the continuation of the experimental work is proposed. In Chapter 2, the main results from the literature study are summarized, with the primary focus on the geochemical behaviour Ti and its fate in natural environments. Chapter 3 provides guidelines for experimental work on Ti-clay interaction within the framework of the KBS-3H disposal concept. In the final Chapter 5, preliminary conclusions are drawn and an outlook for further work is presented.

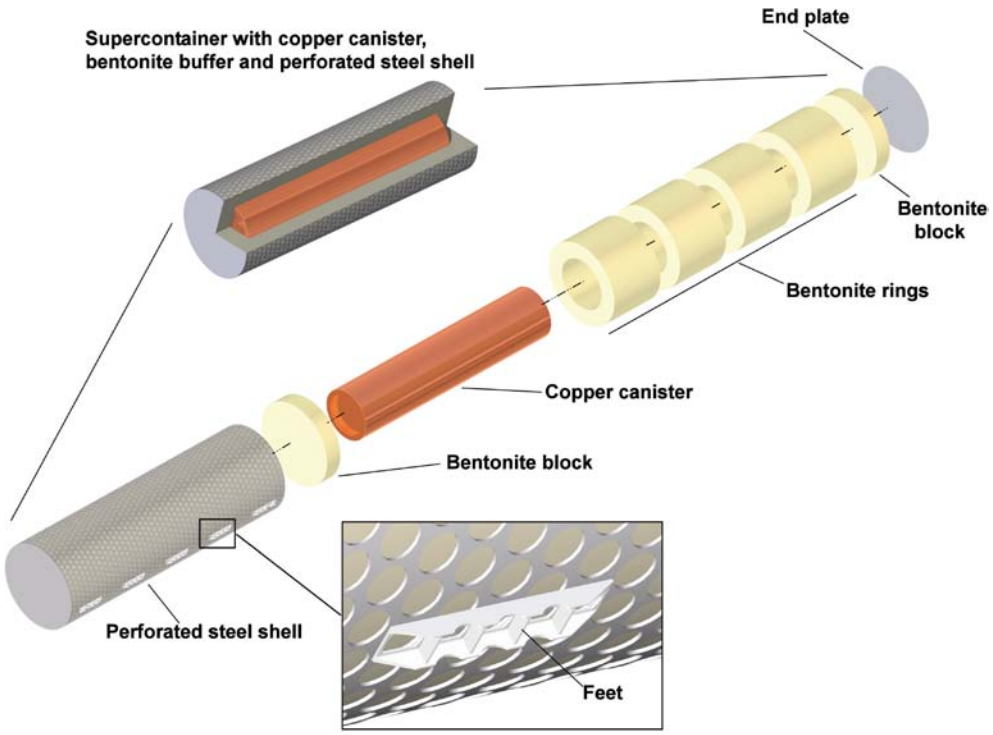

Figure 1-1. *Supercontainer shell design in the KBS-3H concept (SKB 2008).*

2 Geochemical background information

2.1 General considerations

From thermodynamic considerations, metallic Ti is unstable in water. Under most environments on earth, TiO_2 is thermodynamically stable. This can be illustrated in a pe-pH diagram (Figure 2-1). Thus, tetravalent Ti covers a large range of pH and redox conditions. Note that trivalent Ti is thermodynamically not stable in most environments. The main species is TiO_2 in low temperature environments where it may be present as gel (X-ray amorphous) phase, or as mineral phases anatase, rutile and sometimes as brookite. The conversion from anatase to rutile may occur at relatively low temperatures (~50°C). The solubility of all TiO_2 phases is low, as depicted in Figure 2-2 for anatase. In the ranges expected for repository conditions, the solubility of anatase is about 10^{-9} M. Increased solubility (amphoteric behaviour) is noted under acidic and alkaline conditions[1].

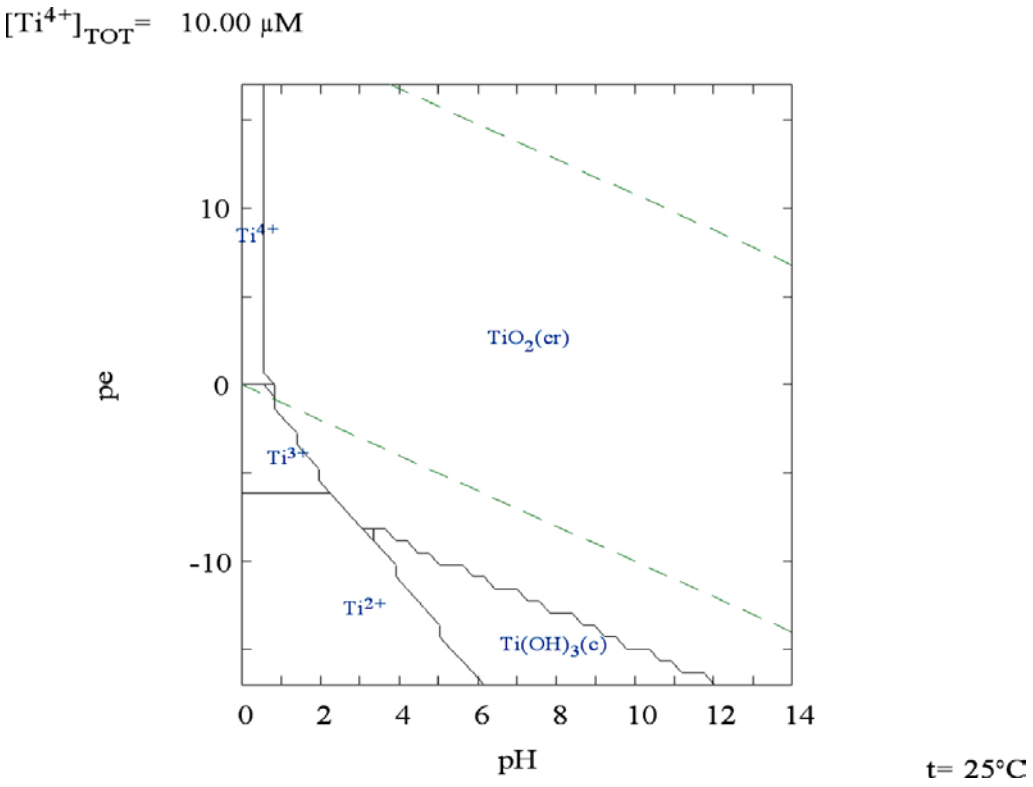

Figure 2-1. *pe-pH diagram of Ti-H_2O system taking thermodynamic data (data taken from HYDRA program, Puigdomenech 2004).*

[1] The thermodynamic data for alkaline conditions are uncertain.

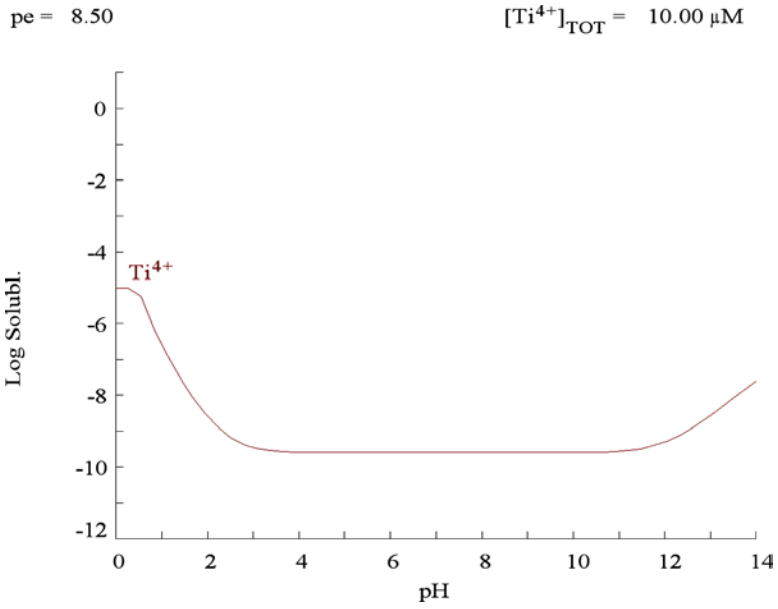

Figure 2-2. *Solubility of TiO_2 (anatase) as function of pH (thermodynamic data, Figure 2-1).*

2.2 Corrosion

There exists a large body of literature on the corrosion behaviour of Ti and Ti alloys. Comprehensive reviews on this topic are given for example by Schutz (2005) and Hua et al. (2004). Table 2-1 gives representative data on corrosion rates under variety of conditions.

This illustrates that corrosion rates are very low (1-20 nm/a), which is a factor of 100 – 1,000 lower than those of steel under anaerobic conditions. This is explained by the rapid build up of a passive TiO_2 film on Ti (e.g. Schutz 2005). This in turn favours localized corrosion and hence crevice corrosion. But, as pointed out by King (2007), life times of Ti Grade 2 fuel containers of 6.35 mm thickness subject to crevice corrosion are of the order of 1,000 – 7,000 years. Thus, premature failure of a Ti supercontainer shell prior to tunnel enclosure is unlikely. Ti is also prone to hydrogen induced cracking, since hydrogen is absorbed during passive corrosion. Predicted lifetimes of Ti structures under repository conditions are 1,000–10,000 years.

Recent electrochemical corrosion studies on Ti in solution and bentonite suspensions have been conducted by a Japanese group. From experiments carried out under neutral anoxic and weakly alkaline conditions at two different temperatures up to 20 weeks of exposure time, it was deduced that an anodic oxide film formed in all samples, which however was “unstable” at higher temperature (80°C), especially in the bentonite suspension (Azumi et al. 2000). A later electrochemical study (Azumi and Seo 2003) - using combined carbon steel-Ti-clad samples - indicated galvanic coupling between Ti and Fe, resulting in a significantly higher anodic corrosion rate at the Fe side, whereas at the cathodic side, the TiO_2 passive layer was affected.

Table 2-1. Selected corrosion rates of Ti and Ti alloys.

Alloy	Environment	Temperature	Corrosion rate	Reference
unalloyed Ti	seawater, aerobic	ambient	0.8 nm/a	Schutz 2005
unalloyed Ti	seawater, aerobic	ambient	<0.25 µm/a	Schutz 2005
Ti Grade 2	simulated groundwater, anaerobic	95°C	~1 nm/a	calc. from Mattsson and Olefjord 1984
Ti Grade 2	bentonite, anaerobic	95°C	~1 nm/a	calc. from Mattsson and Olefjord 1984
Ti Grade 7	conc. brine, aerobic	60 & 90°C	20 nm/a	Hua et al. 2004

2.3 Fate and mobility

Titanium is considered as one of the most inert elements on the earth's surface. Thus, for example Ti is used as reference element in calculating weathering rates of rocks (e.g. Nesbitt 1979, Eggleton et al. 1987). The very low mobility during geological times is evidenced in the presence of Ti beach sands (e.g. Roy 1999).

Tilley and Eggleton (2005) investigated the low temperature weathering of titanite (a common Ti silicate) in a deep seated metamorphic rock. The results showed that the weathered Ti had reacted to form anatase within close vicinity of the altered mineral and thus indicating extremely low Ti migration since weathering.

The mobility of Ti was investigated in a tropical soil by Cornu et al. (1999). It was found that under certain conditions Ti was more mobile than expected and can be transported within centrimetric or even profile scale.

2.4 Occurrence of Ti in clay environments

Authigenic titanium in sediments forms from alteration of Ti-rich high temperature minerals, mainly biotite and ilmenite. Formation products are various forms of TiO_2 (anatase, rutile, brookite, X-ray amorphous TiO_2) and titanite (ideal formula: $CaTiSiO_5$). Morad and Aldahan (1982) reported the authigenic formation of anatase, brookite, rutile and titanite in two old sedimentary rocks. Rutile and titanite were found to occur at higher temperatures and pressures than the other mineral forms in one of the investigated sedimentary sequence.

The low temperature alteration of titanite in a mined metamorphic rock resulted in the formation of beidellite and anatase (Tilley and Eggleton 2005). The mobility of Ti in this rock was reported to be limited to about 0.5 μm (see above).

In soils, Ti occurs mainly in various TiO_2 forms or as co-precipitate with Fe(III) (Fitzpatrick et al. 1978). Common mixed Fe-Ti oxides are titanomaghemite, titanohematite, pseudorutile or pseudo-brookite. They derive from the alteration of primary minerals, such as titanomagnetite or ilmenite.

Titanium is often found to be enriched in kaolinitic materials. Therein, it has been reported to occur in the clay structure by replacing Al or Si (e.g. Maeds and Malden 1975, Rengasamy 1976, Weaver 1976) or associated as TiO_2 (e.g. Jepson 1988, Malengreau et al. 1995, Schroeder and Shiflet 2000). Based on diffuse reflectance spectroscopy, Malengreau et al. (1995) showed the presence of Ti-gels occluded in various kaolinitic materials and questioned the substitution of Ti for structural Al in most kaolinites.

Ti occurs at relatively high levels in bentonite materials. As illustrated in Table 2-2 for representative samples, Ti contents are about 0.1% as TiO_2 (≈600 ppm Ti) for Wyoming bentonites, both in the raw bentonite and the purified homo-ionic clay fraction of <2μm (see Karnland et al. 2006, Vogt and Köster 1978 for purification procedures). In other bentonites, Ti contents can be significantly higher. Thus, for the Rokle bentonite, Karnland et al. (2006) measured about 5% of TiO_2 (≈30,000 ppm Ti) in the purified clay fraction. Anatase was identified by XRD analysis in most samples in the study of Karnland et al. (2006). It is however very difficult to attribute the relative amounts of Ti to Ti species in bentonite, as pointed out by Karnland et al. (2006). The Ti content of the purified clay fraction Ti content in the smectitic fraction is often attributed to the octahedral layer. To our knowledge, spectroscopic evidence for the presence of structural Ti in bentonites is lacking so far. On the other hand, it seems generally accepted that Ti in clays often occurs as rutile or anatase micro-inclusions (e.g. Meunier 2005, p 92).

Synthesized Ti pillared clays have received considerable attention in view of their favourable catalytic properties (Sterte 1986, Jalava et al. 2000). They are constituted of smectite units with intercalated TiO_2. Ti pillared clays are generally synthesized by addition of acidic Ti solution to the smectite material, followed by high-temperature calcination. This produces cross-linked or pillared polymeric titania units in the smectite interlayers with relative large and thermally stable pore sizes (Romero et al. 2006).

Table 2-2. Ti contents (expressed as wt % TiO2) in some bentonite materials.

Bentonite	TiO_2 (%) raw material	TiO_2 (%) purified clay	Reference
Upton Wyoming sample	0.11	0.11	Vogt and Köster 1978
Clay Spur Wyoming sample	0.12	0.11	Vogt and Köster 1978
Wyoming samples	0.1–0.2	0.1	Karnland et al. 2006
Milos samples	0.7	0.7	Karnland et al. 2006
Asha samples	0.8–1.9	0.4–1.4	Karnland et al. 2006
Rokle sample	4.1	4.8	Karnland et al. 2006

2.5 Experimental studies in clay environments

Very few experimental investigations on Ti-clay systems have been carried out so far. The Japanese electrochemical studies involving bentonite suspensions have been summarized in Section 2.2.

The main part of experimental studies on this topic known to us are those performed in the 1980ies by the team of Prof. Olefjord at Chalmers (S) as part of SKB's corrosion program (Mattsson and Olefjord 1984, 1990, Mattsson et al. 1990). The corrosion of Ti was studied in simulated groundwater and in compacted bentonite at 95°C for time periods up to six years. The analytical technique was X-ray photoelectron spectroscopy (XPS) combined with ion sputtering. The film growth was found to be same in solution and compacted bentonite and independent of ionic strength and the composition of the Ti alloy. A logarithmic rate law (Eq-1) was determined from the observed TiO_2 film thickness:

$$y = 71.7 + 3.65 \cdot \ln(t) \qquad \text{(Eq-1)}$$

where y is the film thickness in Å. The film thickness after five years was about 6–9 nm. The increasing corrosion rate with time was interpreted as a result of recrystallisation of TiO_2 (am) to anatase of the Ti corrosion products, leading to facilitated pathway for Ti along grain boundaries. The overall corrosion rate was very low, in the range of 1 nm/a (see above). No difference in rates between clay-free and bentonite exposed Ti samples was noted. A side result from the studies of Mattson & Olefjord was that the only Ti species determined in the clay matrix was TiO_2, although this aspect was not studied in detail.

3 Consequences for titanium-clay interaction studies

3.1 Objectives for titanium-clay interaction studies

The primary objective is to demonstrate that the Ti alloy supercontainer shell material will not adversely affect the buffer's safety functions to any significant extent. An important aspect of this demonstration exercise is to describe the corrosion and potential interaction processes with the clay.

Because of the low corrosion rates and low solubility of Ti^{4+}, only limited reactivity with the clay and thus small amount of reaction products can be expected. Furthermore, the rather high Ti content in the "pristine" clay complicates the analysis of reacted Ti species.

3.2 Possible Ti species resulting from Ti-smectite interaction

In principle, the interaction of elemental Ti with smectite may result in the following possible reaction products:

- Ti sorbed to the clay by cation exchange or specific sorption to edge sites
- Ti polymerized as cross-linked TiO_2 units in the interlayer (Ti pillared clay)
- Ti incorporated in the octahedral or tetrahedral clay structure
- Ti precipitated as separate TiO_2, Ti-Fe oxide or Ti-silicate phase

From the available (rather scarce) literature information and the very low solubility of TiO_2 the most likely reaction product is TiO_2. On the other hand, the formation of pillared Ti units in the interlayer under the expected conditions is highly unlikely, given the complete lack of such a mineral form in nature. The formation of a Ti-silicate phase, such as titanite under low temperature conditions is also not expected. These latter two reaction pathways would be the most adverse for the safety functions of the buffer. Table 3-1 presents the likelihood of Ti reaction products and their qualitative effect on buffer stability.

Table 3-1. Possible Ti species resulting from Ti-clay interaction.

Formed Ti species	Likelihood of reaction	Impact for buffer stability
Sorbed Ti(IV)	high	low
Precipitated TiO_2 or mixed (Ti, Fe) oxide	high	low
Precipitated Ti-silicate	low	high
Incorporated in clay structure	medium	low–medium
Ti pillared clay (TiO_2 in interlayer)	very low	high

3.3 Experimental challenges and ways to resolve these

From the information presented above, it becomes clear that the amount of reacting Ti with the clay will be small and the "influence" range will be very limited. Furthermore, natural bentonite materials contain considerable amounts of "background" Ti. This puts considerable constraints on meaningful experimental work, designed to study effects of Ti-clay interactions on the clay properties. It requires well characterized, purified smectite starting material with low Ti content.

The main experimental challenge results from the low corrosion rate and solubility of Ti. In order conduct short term experiments on the Ti-clay interaction processes which may be relevant at large timescales, the corrosion process needs to be speeded up. This, in principle can be done by adjusting the following parameters:

- increase in reactive metallic surface area
- increase in temperature
- adjustment of pH to acidic or alkaline conditions

The analysis of the spatially very limited range of Ti reacted with clay requires sophisticated spectroscopic tools and an experienced spectroscopist in the team. Possible spectroscopic methods which can detect Ti speciation under the conditions expected include XPS and synchrotron-based X-ray absorption spectroscopy (XAS). The correct interpretation hinges on the availability of well-characterized reference materials (TiO_2, structural Ti in the clay, Ti silicate).

4 A preliminary Experimental study

4.1 Scope of study

With a number of pre-tests, in which bentonite materials are exposed to metallic Ti, qualitative information on the Ti-clay interaction process shall be obtained. The main objectives of this preliminary study are:

- Identification of Ti speciation in "pristine" bentonites,
- Identification of reaction products from Ti-bentonite interaction under simulated EBS conditions, i.e. precipitated TiO_2, sorbed Ti, Ti incorporated in clay structure, Ti-silicate precipitate etc.
- Development of experimental methodology for Ti-clay interaction studies and optimization of spectroscopic analysis, and
- Provide the basis for deciding on necessity for further Ti-clay program and, if yes, experimental outline for this program.

The study is done in two steps: In the first step, a series of batch tests under different conditions are set up and run for five months. A part of the tests are then stopped and the solid material and solutes are analyzed. The central analytical part is XAS analysis on reference materials as well as on un-reacted and reacted clay samples. With the results obtained thereof, new batch tests with "optimized" conditions are designed and run in step two. After several months, the next run of tests will be analyzed.

The final results from this pre-study form the basis for deciding on the continuation of the Ti-clay interaction programme.

In this report the data from step 1 are presented.

4.2 First series of batch tests

4.2.1 Starting materials

Ti-bentonite interaction was studied with batch shaking tests. Following materials were used:

Titanium:

- 99.5% purity grade 0.1 mm thick titanium metal foil, or
- 99% purity grade titanium metal nanopowder with the specific surface area of 12 m^2/g from American Elements.

Bentonite:

- MX-80 bentonite, which was fractionated to separate the clay, and homoionized to Na-form according to the purification procedure described in Karnland et al. (2006). Despite of rigorous purification procedure, purified MX-80 contained in addition to smectite, also trace amounts of mineral impurities as well as organic matter (Table 4-1). Titanium was not enriched nor decreased in the clay fraction indicating that it was either structurally bound to montmorillonite or present as clay-sized accessory minerals.

Table 4-1. Chemical composition of initial and purified MX-80 bentonite. Chemical composition was determined with ICP-AES, combustion and gravimetric methods and the results were normalized to 100 wt % excluding the adsorbed water (H2O).

	SiO_2 wt %	Al_2O_3 wt %	Fe_2O_3 wt %	FeO wt %	TiO_2 wt %	MgO wt %	CaO wt %	Na_2O wt %	K_2O wt %	CO_3 wt %	$C_{org.}$ wt %	SO_4 wt %	S_{other} wt %	LOI wt %	H_2O wt %
Initial MX-80	65.37	18.70	3.50	0.36	0.15	2.34	1.29	2.19	0.53	0.79	0.14	0.14	0.20	5.36	9.49
Purified MX-80	65.34	20.20	3.62	0.21	0.14	2.29	0.03	2.73	0.06	0.30	0.10	0.00	0.00	5.39	2.69

4.2.2 Experimental procedure

Purified, oven-dried (60ºC) MX-80 bentonite was ground in agate mortar with a pestle. 2 g of purified and ground bentonite was dispersed in 100 mL of 0.01 M NaCl solution. The pH of suspension was left as it was (bulk), or adjusted with addition of 1 M NaOH or 1 M HCl to pH 12 or pH 2, respectively. Then, the suspension was purged with nitrogen for 30 min. Four types of batch samples were prepared:

- Approximately 2 g of titanium nanopowder were closed inside a Spectrapore 7 dialysis bag, which had been flushed with deionized water and had a porosity of 3 500 MWCO, was added to the bentonite suspension. Dialysis bags were used in order to study the effect of dissolved titanium on smectite and to separate the smectite transformation and titanium corrosion products.
- Titanium foil was etched in 1 M HCl overnight, and quickly rinsed with acetone. Approximately 2 g of foil with the specific surface area of 0.004 m^2/g, were added to the bentonite suspension.
- Approximately 2 g of titanium nanopowder were added to the bentonite suspension without the dialysis bag.
- An empty dialysis bag was added to the bentonite suspension.

After addition of titanium or empty dialysis bags, the suspensions were purged with nitrogen for another 30 minutes. After purging, sample vessels were closed quickly, wrapped in aluminium foil to exclude the effect of light, and placed in a rocking platform shaker. The list of batch samples prepared accordingly is presented in Table 4-2.

After four months, 5 samples were dismantled by taking out the titanium foil or dialysis bag with Ti nanopowder inside. Thereafter, the clay suspensions were centrifuged for 3 h in 4 000 rpm, and the solution was separated from the sedimented clay. Additionally in sample 6, the solution was separated from titanium nanopowder, which sedimented with clay during centrifugation to the bottom of the tube. Wet clay samples were sent to PSI for further analysis.

Solution pH and electric conductivity (EC) was measured after the experiment. Solutions were filtered through a 0.2 µm pore size membrane filter, and analysed for Fe, Na and Ti at Labtium Oy with ICP-AES.

4.2.3 Wet chemistry results

The pH of final solutions of samples without pH adjustment was somewhat decreased (Table 4-3). Titanium concentrations in solution were below or near detection limit (0.02 mg/L).

Table 4-2. Experimental settings for Ti-bentonite batch tests started on 22.9.2008.

Sample number	Label	Ti present	Dialysis bag	pH adjustment	Dismantling date
1	TiNP-C-D-bulk	nanopowder	yes	none	13.1.2009
2	TiNP-C-D-bulk2	nanopowder	yes	none	ongoing
3	TiNP-C-D-pH2	nanopowder	yes	2.0	13.1.2009
4	TiNP-C-D-pH12	nanopowder	yes	12.4	13.1.2009
5	C-D-bulk	none	yes	none	ongoing
6	TiNP-C-bulk	nanopowder	no	none	13.1.2009
7	C-D-pH2	none	yes	2.1	ongoing
8	C-D-pH12	none	yes	12.4	ongoing
9	C-D-bulk2	none	yes	none	ongoing
10	TiFO-C-bulk	foil	no	none	13.1.2009
11	TiFO-C-bulk2	foil	no	none	ongoing
12	TiFO-C-pH2	foil	no	2.1	ongoing
13	TiFO-C-pH12	foil	no	12.5	ongoing
14	TiNP-C-D-bulk3	nanopowder	yes	none	ongoing
15	TiNP-C-D-pH2/2	nanopowder	yes	2.1	ongoing
16	TiNP-C-D-pH12/2	nanopowder	yes	12.4	ongoing

Table 4-3. pH, EC and wet chemistry results for the first set of pre-study batch test samples.

					ICP-AES		
Sample number	Label	Initial pH	Final pH	EC (mS/cm)	Fe (mg/l)	Na (mg/l)	Ti (mg/l)
1.	TiNP-C-D-bulk	~8.7	7.9	1.35	1.84	282	0.06
3.	TiNP-C-D-pH2	2.1	2.8	2.95	3.10	438	<0.02
4.	TiNP-C-D-pH12	12.4	12.2	6.34	<0.3	1,510	0.02
6.	TiNP-C-bulk	~8.7	6.7	1.39	nd	nd	nd
10.	TiFO-C-bulk	~8.7	7.4	1.32	nd	nd	nd

Abbreviations: nd = not determined

4.3 Spectroscopic analysis of first experimental series

4.3.1 Experimental

The samples being studied are presented in Table 4-4. The elemental composition of the different clay samples – with special emphasis on Ti content – were analysed by synchrotron-based X-Ray Fluorescence (XRF) analysis as well as X-ray tube based quantitative XRF analysis.

The synchrotron-based XAS investigations reported here were conducted at the microXAS Beamline (X05LA) of the Swiss Light Source (SLS), Paul Scherrer Institute, Villigen Switzerland. Typical operation conditions of the SLS were 2.4 GeV and 400 mA current (top-up mode). The microprobe beamline X05LA is an insertion device beamline dedicated to X-ray microbeam applications in materials and environmental sciences. The X-ray microbeam is obtained by directly imaging the source by means of two elliptical mirrors aligned in a classical Kirkpatrick-Baez arrangement. However, during the present XRF measurements the beam was defocused to produce a large beam foot-print on the sample. By illuminating a larger sample area, typical artefacts due to sample inhomogeneity can be limited. The X-ray beam was monochromatized by a fixed-exit double crystal monochromator using a pair of Si [111] crystals. Energy calibrations were carried out using standard metal foils measured in transmission. Fluorescence emission was recorded using a single element Silicon Drift Diode (SDD) detector.

Using synchrotron-based XRF, two types of samples were investigated: i) wet pastes and ii) dried samples. However, due to time constraints, measurements were performed without matrix-matched reference standards accordingly yielding semiquantitative results. Despite being only semi-quantitative, a relative comparison of elemental concentrations within a consistent data set (as recorded in the present campaign) is still valid and meaningful.

In addition to the synchrotron-based XRF measurements, laboratory source based macro X-ray fluorescence (macroXRF, Spectro X-LAB 2000 Kleve, Germany) analysis was employed. Based on the fundamental parameter approach, these kinds of measurements yield quantitative results.

Important to note: The impact of Ti corrosion product loadings on the physical and chemical properties of clay barriers does not exclusively depend on the absolute quantity of Ti loading. Of most importance is the chemical form Ti ending up in the clay material. Accordingly, there is need for analytical tools capable in providing this kind of molecular level information. Extended X-ray Absorption Fine Structure (EXAFS) spectroscopy corresponds to an analytical technique able to identify the local atomic geometry around a given atom. EXAFS analysis can provide reliable measure of the identity of neighbouring atoms and related local interatomic distances with good accuracy. Consequently, Ti K-edge EXAFS spectra were collected to determine the predominant chemical speciation of Ti within the different clay samples. Bulk EXAFS measurements have been recorded at the microXAS beamline at the Swiss Light Source. Ti K-edge EXAFS spectra were recorded in fluorescence mode.

Validation experimental methodology

MX-80 corresponds to the primary material of interest of the present investigations. However, additional natural clay materials have been analysed by XRF. XRF measurements are yielding characteristic fluorescence lines which can be assigned uniquely to chemical elements (Figure 4-1). The primary purpose of these initial investigations was to determine the relative concentration of Ti within different clay materials and to identify the detection limits of Ti fluorescence concerning X-ray absorption techniques (XANES, EXAFS).

Table 4-4. Samples for spectroscopic analyses.

Reference material	Experimental details
Titanite	$CaTiSiO_5$, provenance Parainen, Finland
Ti Nanopowder	Reacted nanopowder: see sample 3, TiNP-C-D-pH2, below
Rutile	TiO_2
Anatase	TiO_2
Ti(0)	Ti metal foil
Rokle Clay	Natural Clay material
Illite de Pully	Natural Clay material
Opalinus Clay	Natural Clay material
MX-80	Natural Clay material
MX-80 purified	Natural Clay material, purified
Sample Number/Label	**Sample description, experimental details**
1. TiNP-C-D-bulk	Ti-nanopowder –purified MX-80 mixture, without pH adjustment, Ti in dialysis bag, removed
3. TiNP-C-D-pH2	Ti-nanopowder – purified MX-80 mixture pH initially adjusted to 2, Ti in dialysis bag, removed
4. TiNP-C-D-pH12	Ti-nanopowder – purified MX-80 mixture, pH initially adjusted to 12, Ti in dialysis bag, removed
6. TiNP-C-bulk	Ti-nanopowder – purified MX-80 mixture without pH adjustment, Ti-nanopowder mixed with clay and present in the end product
10. TiFO-C-bulk	Ti-foil – purified MX-80 mixture, without pH adjustment, Ti-foil removed

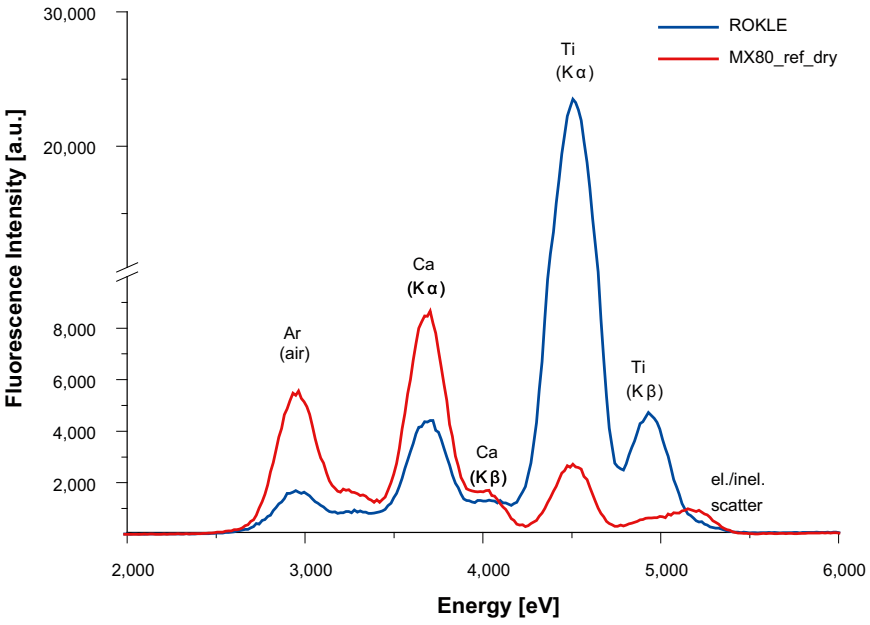

Figure 4-1. *Ca and Ti content of different clay materials. The semi-quantitative XRF analysis yields an approximately ten-fold higher Ti concentration in the Rokle Clay compared to the MX-80 clay material.*

Figure 4-1 shows a comparison of the MX-80 clay material with the natural ROKLE clay. By choosing an excitation energy of 5.25 keV, the analysis is limited to chemical elements with $Z \leq 22$ (Ti). For the untreated MX-80, a clear signal originating from geogenic Ti can be detected. At this point an important concern should be mentioned: The intrinsic Ti content of the MX-80 clay can be expected to result in difficulties to characterize additional Ti loadings originating from the proposed corrosion experiments.

Compared to the MX-80, the ROKLE clay yields even higher geogenic Ti background content. Based on the semi-quantitative XRF analysis shown in Figure 4-1, an increase in the order of approximately a factor of 40 is expected. Similarly, the Ca content in the ROKLE clay material is elevated by a factor of about two.

Efficiency of the washing procedure

As mentioned above, the significant geogenic Ti content of the MX-80 primary material will potentially mask the 'anthropogenic' Ti originating from the corrosion of metallic Ti present in the vicinity of the clay. Consequently, a chemical treatment was proposed and applied in order to remove the geogenic Ti prior to the corrosion studies. However, as can readily be seen from Figure 4-2, the applied purification treatment was not effective with respect to Ti. Within the uncertainty of the employed XRF analysis, the Ti concentration remains unchanged. Ti in its geogenic form was not dissolved and could not be removed. In contrast, a significant reduction in the Ca content can be established. Most likely, the chemical treatment resulted in the dissolution of Ca-carbonate and/or Ca-sulphate species and subsequent removal of the dissolved Ca-ions.

Ti Transfer

Different purified MX-80 samples were exposed to corroding metallic Ti under varying chemical conditions. The primary objective of the corresponding XRF analysis was to determine the amount of Ti released by the corrosion processes and subsequently being trapped by the clay material. As illustrated in Figure 4-3, neither of the applied corrosion procedures results in a measurable net flux of Ti from the source (corroding metallic Ti) to the proposed sink (clay material), despite the extreme chemical conditions. Measured Ti fluorescence intensities are in neither case exceeding the signal for the unexposed reference material. For the material exposed under basic conditions (pH 12), the XRF measurements yield even lower Ti intensities. This is indicative of the removal of geogenic Ti over the course of the experiment.

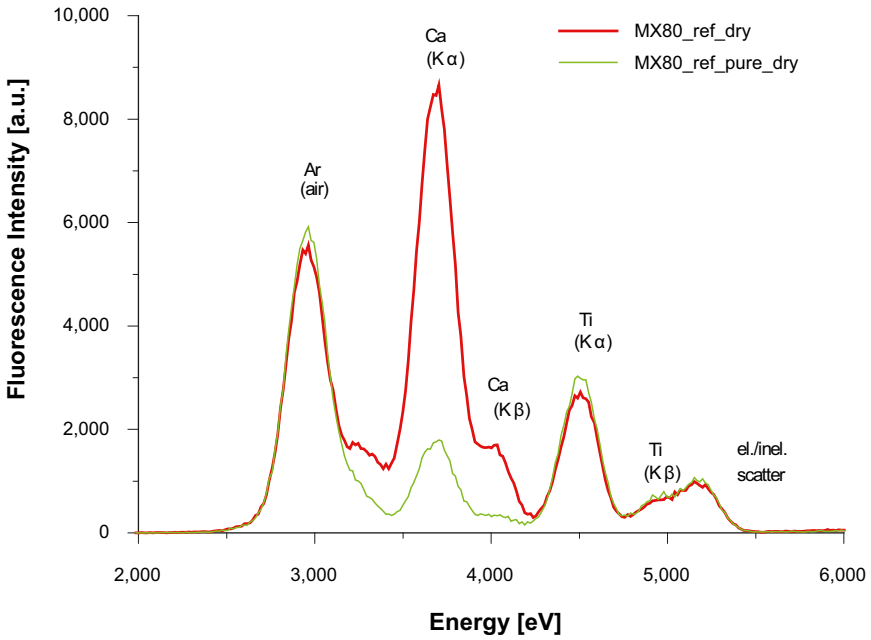

Figure 4-2. *Effectiveness of the employed purification procedure. Despite the intensive conditioning procedure the Ti content remained unchanged. However, a clear reduction in the Ca content can be established (removal of $CaCO_3$ and $CaSO_4$).*

Quantification Quality control: quantitative XRF

In order to validate the semi-quantitative results obtained by synchrotron-based XRF, independent measurements were conducted. These investigations were based on quantitative XRF analysis using a laboratory based X-ray tube. Quantification was based on internal standards and the fundamental parameter approach to minimize matrix effects.

First, quantitative XRF confirmed the differences in Ti concentrations between MX-80 and Rokle Clay observed previously. The approximately 40-fold difference obtained by the semi-quantitative synchrotron XRF method is reproduced. However, quantitative values can now be provided as well. Rokle Clay contains about 2.3 weight-percent Ti, while only 0.055 are found in the MX-80. (For a full comparison, see Appendix).

Of central interest was to verify the observed variations of the ingress and efflux of Ti under varying chemical conditions. Unfortunately, the highly limited amount of available sample mass turned out to be a severely limiting obstacle regarding accurate quantification. The available mass of clay material had to be diluted by a factor of ~10 in order to be physically able to prepare appropriate sample pellets. However, as a consequence of this dilution, several analytical problems have arisen. Examples include: the low concentration was further diluted becoming close to detection limits, difficulties to achieve a homogeneous mixing, samples and internal standards were no more matrixmatched, etc. Due to the severely limited accuracy, the only firm conclusion is that the clay samples exposed to Ti corrosion did *not* show an elevated Ti content.

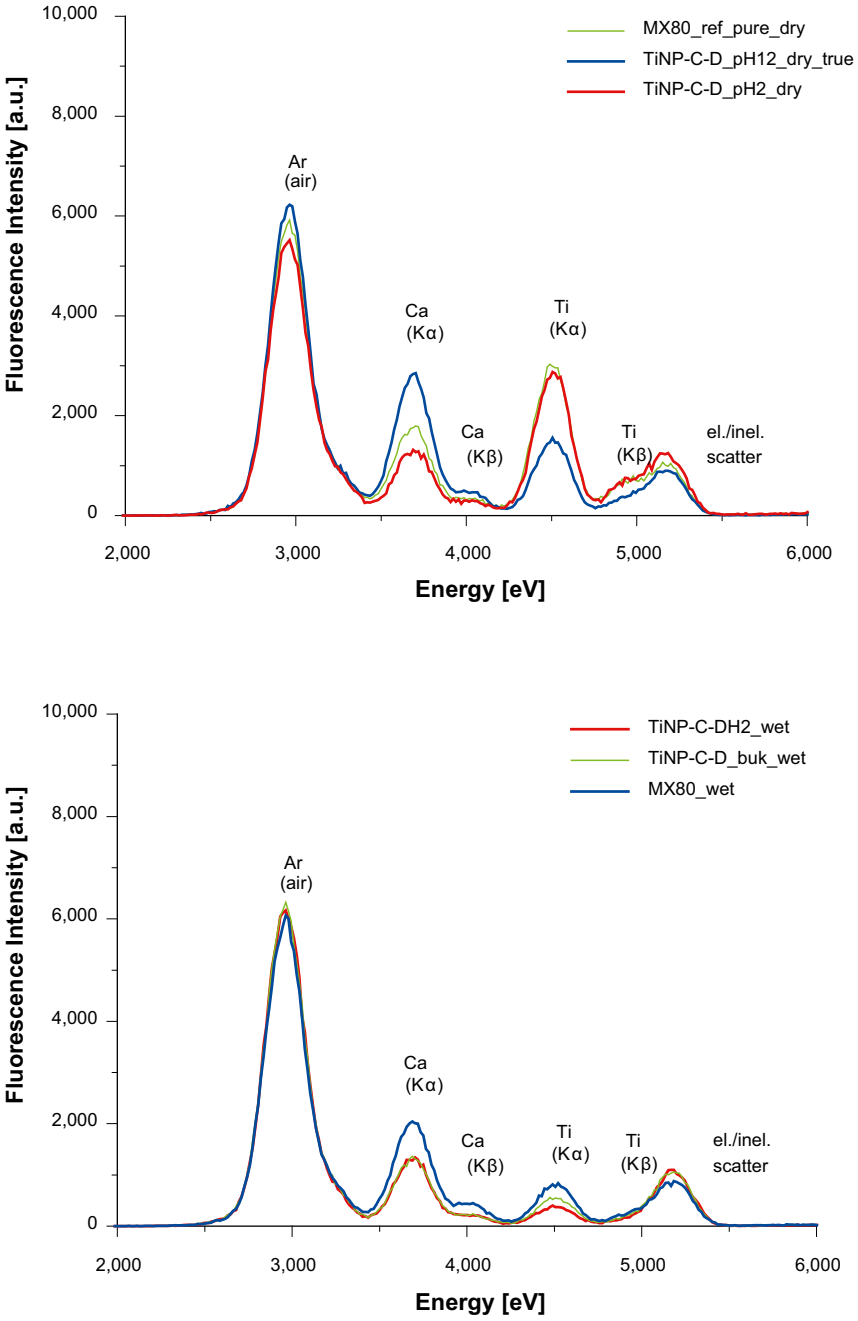

Figure 4-3. *Quantification of the Ti transfer flux. XRF analysis was performed on dry clay materials (top) and wet pastes (bottom). No net flux from the Ti source to the clay material can be observed.*

4.3.2 Feasibility study concerning Ti molecular-level speciation in clay materials

The following feasibility study is directed towards understanding fundamental chemical (molecular) aspects of the Ti-clay interaction. Measurements and results presented so far are covering quantitative aspects only. However, in order to understand the impact of ingressing Ti on the stability and reactivity of clay barriers, a molecular-level understanding of the Ti speciation is crucial. The primary objective was to compare the chemical nature of the anthropogenic Ti to the molecular structure Ti of geological origin.

In principle, the interaction of Ti corrosion products with clay materials may result in the following possible reaction products (Section 3.2):

- Ti sorbed to the clay by cation exchange or specific sorption to edge sites
- Ti incorporated in the octahedral or tetrahedral clay structure
- Ti precipitated as separate TiO_2, Ti-Fe oxide or Ti-silicate phase
- Ti polymerized as crosslinked TiO_2 units in the interlayer (Ti pillared clay)

Ti X-ray Absorption spectroscopy

Extended Fine Structure Spectroscopy (EXAFS): Model substances metallic Ti and Ti nanoparticles

As a basic test of Ti X-ray absorption spectroscopy (XAS), metallic Ti and Ti nanoparticles were analysed by XAS. As can be seen in Figure 4-4, a clear and clean spectroscopic signal of high quality is obtained for metallic Ti. The observed oscillating pattern is originating from interferences of the molecular cluster around each Ti atom. The pattern obtained for the Ti nanoparticles illustrates the outstanding sensitivity of XAS to determine the structure of molecular clusters. The core of the Ti nanoparticle has a similar 'crystallographic' signature as bulk metallic Ti resulting in a congruent basic EXAFS pattern (Figure 4-4). At the outer surface of the nanoparticle, however, Ti is coordinatively undersaturated. This explains the reduced amplitude and increased broadening of the EXAFS signal. (A more detailed analysis of the EXAFS spectrum would allow determining the Ti coordination at the surface of the nanoparticles.)

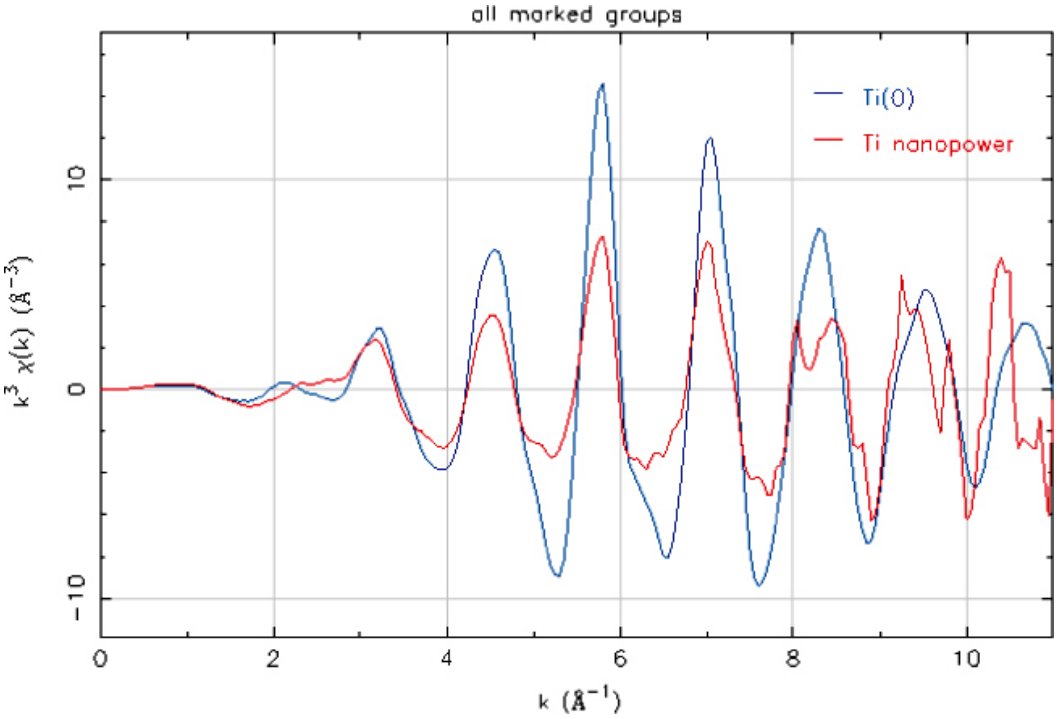

Figure 4-4. *Ti nano-powder similar to metallic Ti, but additional contribution from surface shell visible (incomplete coordination of Ti in the surface layers of the nanoparticles).*

Near Edge Spectroscopy (XANES): Ti-Oxides (TiO_2)

Features before the absorption edge arise due to inner-atomic transitions (Figure 4-5). Core shell electrons are excited to unoccupied valence shell orbitals. At excitation energies slightly above the edge, multiple scattering from neighbouring atoms dominates the signal. Consequently, XANES is probing the local electronic and coordinative structure of molecular clusters.

The sensitivity of the XANES technique is demonstrated by comparing the spectral features from the two polymorph forms of TiO_2, rutile and anatase. Pre-edge features and edge structure are clearly different (Figure 4-6). Despite the identical chemical composition, the small differences in molecular structure (Figure 4-7) can be resolved.

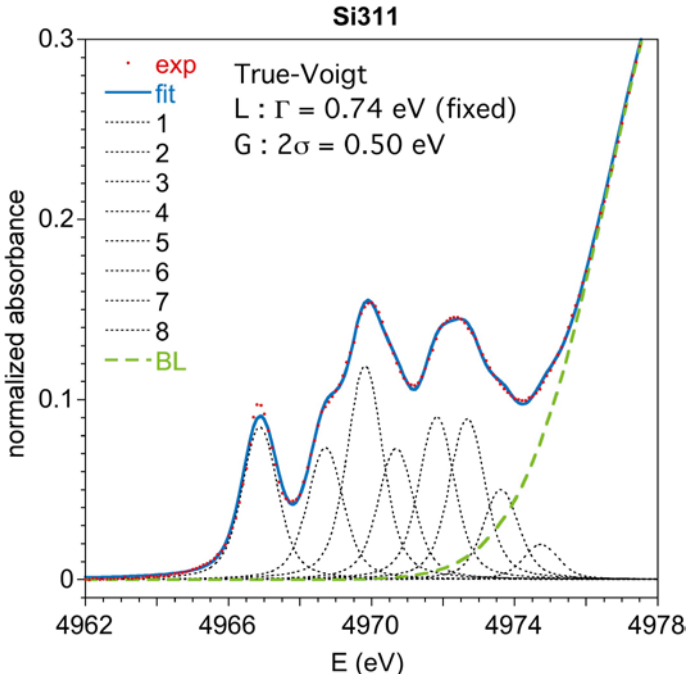

Figure 4-5. *Pre-edge structure of Ti. The pre-edge features at the Ti K-edge are indicative of the local electronic and coordinative structure of the Ti bonding environment. As an example, Figure 4-5 depicts the pre-edge structure of TiO2 (anatase form) including convolution.*

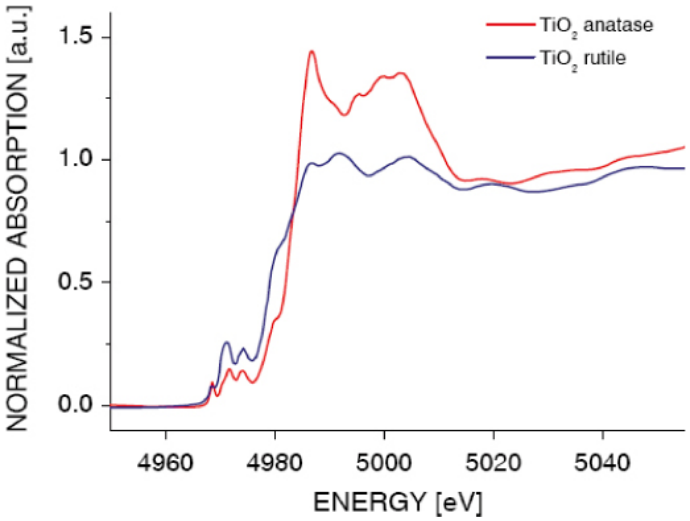

Figure 4-6. *Pre-edge structure of Ti. Pre-edge features allow identifying ('fingerprint') different Ti bonding environments, e.g. the two polymorph TiO_2 forms anatase and rutile.*

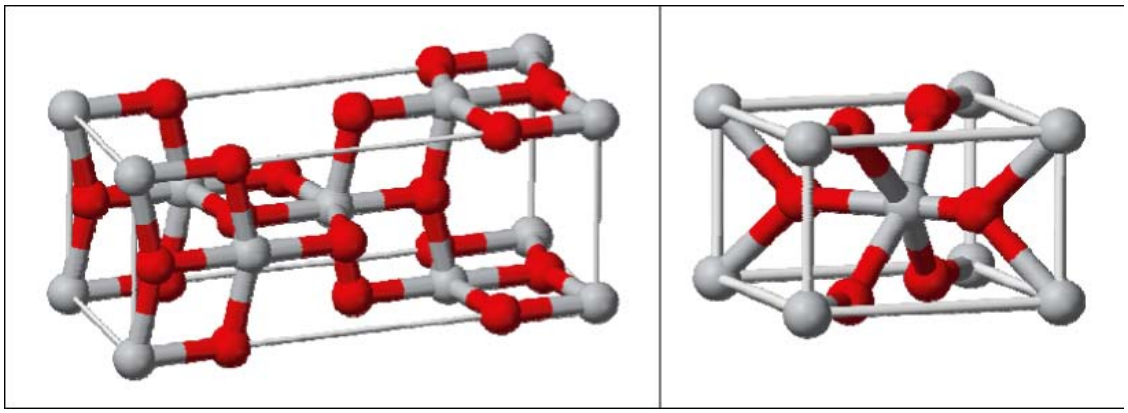

Figure 4-7. *Unit cell structure of the two polymorph TiO_2 forms anatase (right) and rutile (left).*

Molecular environment of Ti in natural clays

Rokle Clay

In Figure 4-8, the XANES spectrum of the Rokle Clay is compared to the reference spectrum of TiO_2 (anatase). The two spectra are nearly identical. Based on this observation one can conclude that the chemical speciation of the Ti in the Rokle clay is predominately like TiO_2 (anatase). This conclusion is further supported by local molecular structure analysis by means of EXAFS spectroscopy (Figure 4-9). The spectroscopic signature of Ti in Rokle clay is in convincing agreement with the spectrum of TiO_2 (anatase).

Opalinus Clay

In Figures 4-10 and 4-11, Opalinus Clay is also included in the comparison. For Opalinus clay, the Ti speciation is again alike TiO_2 (anatase). Considering the pronounced sensitivity of the pre-edge transitions to the bonding structure, it is quite remarkable, how close the pre-edge features for these two natural clay materials match the crystalline TiO_2 (anatase). Only a slightly increased disorder can be extracted from the EXAFS spectra. One may concludes that in these two natural clay materials, the major fraction of Ti is not incorporated in the clay structure, but present as (nano) crystalline TiO_2 (surface) precipitates.

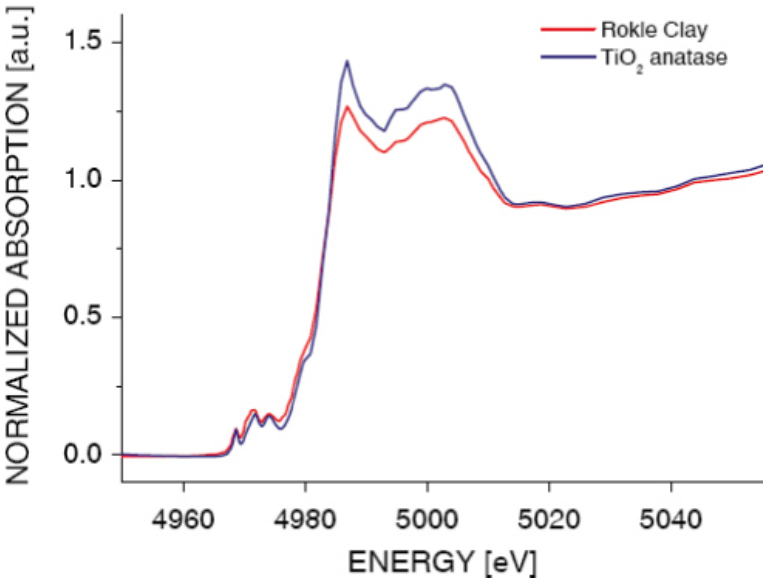

Figure 4-8. *Based on fingerprinting of the pre-edge features at the Ti K-edge the coordination observed in the Rokle Clay material turns out to be nearly identical with TiO2 (anatase form).*

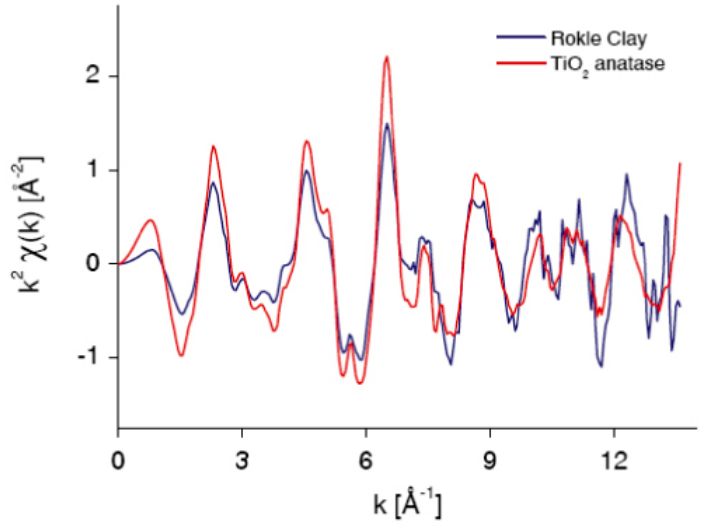

Figure 4-9. *'Empirical' fingerprinting shown in Figure 4-8 is strongly supported by molecular structure analysis by means of EXAFS spectroscopy. EXAFS yields the molecular environment of Ti. The molecular structure observed for Ti in Rokle is similar to TiO_2 (anatase).*

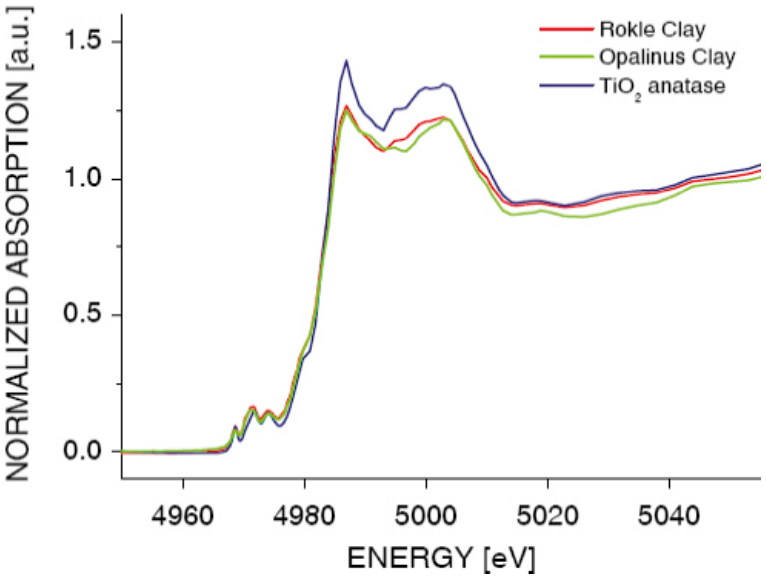

Figure 4-10. *Ti XANES of two natural Ti-clay materials (Rokle Clay, Opalinus clay) compared to anatase TiO_2. Remarkable is the close match of the pre-edge features.*

MX-80 Clay, Illite du Pully

For MX-80 and Illite du Pully the structural bonding seems to be different. Comparing the XANES depicted in Figure 4-12 with the TiO_2 (anatase) reference shown in Figure 4-10, distinct differences are readily apparent. Most prominent, the pre-edge features of MX-80 and Illite du Pully are reduced to one dominated transition. The post-edge features are considerably smoother. The Ti speciation observed in MX-80 and Illite du Pully resembles the Ti coordination environment found in CaTiSiO5 (titanite). This represents an indication that Ti is incorporated in the clay structure. Detailed XANES and EXAFS simulations would be required to confirm this hypothesis, however.

Note: Due to the low geogenic Ti concentration in MX-80 and the presence of significant spectroscopic interferences due to impurities in MX-80 the quality of the presented spectra is limited.

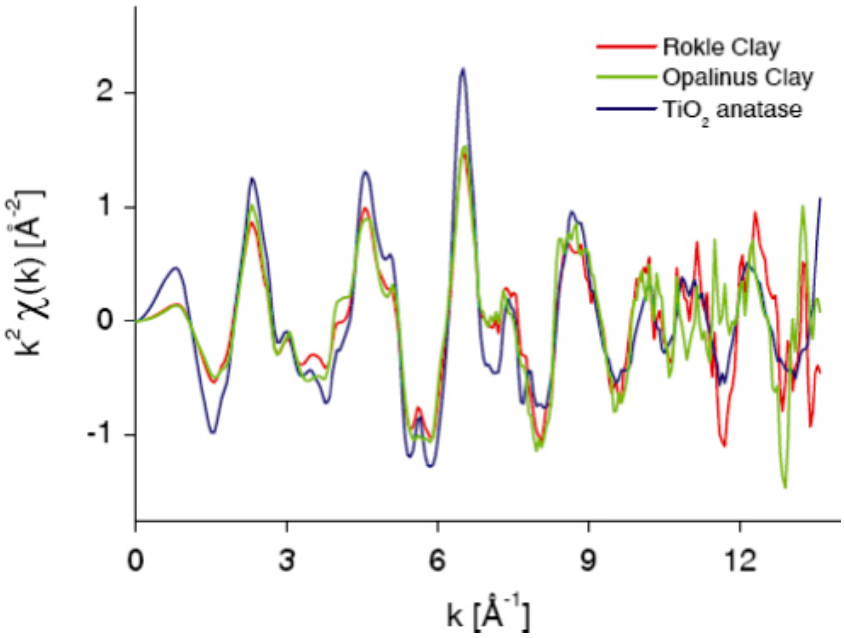

Figure 4-11. *Ti EXAFS of two natural Ti-clay materials (Rokle Clay, Opalinus clay) compared to anatase TiO_2. The reduced amplitude of the spectra for the two natural materials points to an increased degree of disorder as compared to pure crystalline TiO_2 (anatase). In the natural clay materials, Ti is most likely present in the form of small TiO_2 anatase nanoparticles.*

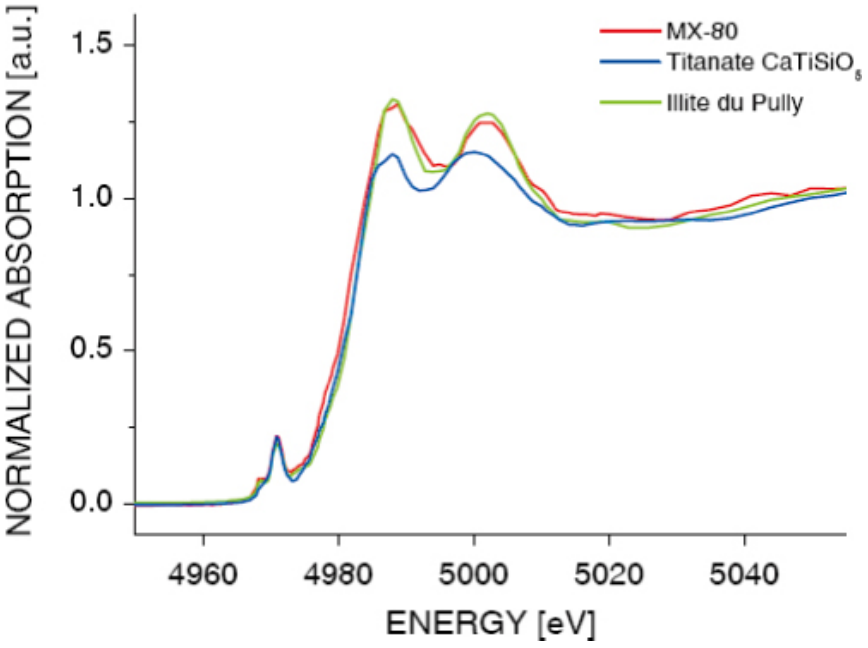

Figure 4-12. *The speciation of Ti in MX-80 and Illite du Pully seems to deviate from the previously discussed clay systems. Both, the pre-edge structure and the post edge features point towards a bonding environment different than TiO_2.*

4.3.3 Summary from spectroscopic analysis

The results of the present quantification and spectroscopic investigations can be summarized as follows:

First, a considerable geogenic Ti background concentration was found in the MX-80 clay material. This represents a severe obstacle regarding the proposed investigations focusing on clay – Ti interactions. The background signal will contribute and may even mask the response of supplemented Ti. Without initial removal of the geogenic Ti, the geochemistry of corrosion-derived Ti cannot be traced down unambiguously.

Second, the applied purification procedure aiming to remove the geogenic Ti background was not effective.

Third, the corrosion of metallic Ti in the vicinity of MX-80 clay for an extended period of time (4 months) did not result in elevated Ti contents in the clay material.

Finally, we could successfully demonstrate having means to determine the Ti speciation in various clay materials. However, for lower Ti concentrations and, in case of interferences, advanced analytical strategies may be required.

4.3.4 Proposed next steps

The main premise for obtaining reliable spectroscopic data on Ti-clay interactions is to use smectite materials with a very low Ti content. Thus, synthetic "Ti-free" montmorillonite is proposed as starting material. This material will be analyzed after reaction with metallic Ti, both in terms of Ti speciation in the clay and the corrosion layer at the metal surface.

Spectroscopic analyses of Ti speciation in the clay include:

- XANES and EXAFS spectroscopy on various natural clay materials and synthesized Ti pillared clays (to allow fingerprinting of exposed clay)
- MicroXRF / microXRD for investigating micro-domains, the possible presence of Ti-gels and of crystalline Ti species (e.g. Fe-rich compounds).

Analyses of the corrosion layer of metallic Ti include:

- XANES/EXAFS spectroscopy
- Reflectivity measurements
- MicroXProbe analysis.

4.4 Second series of batch tests

Ti-bentonite interaction was studied with a very similar setup as was used for the 1st series. The main difference was the use of synthetic "Ti-free" montmorillonite instead of purified MX-80 and the increase in temperature to 80°C. The scope was to accelerate Ti corrosion on one hand and decrease the background Ti concentrations in the clay on the other. The materials are described in short below:

4.4.1 Starting materials

Titanium:

- 99.5% purity grade 0.1 mm thick titanium metal foil, or
- 99% purity grade titanium metal nanopowder with the specific surface area of 12 m^2/g from American Elements.

Synthetic montmorillonite:
Na-montmorillonite synthesis (sample ACF3141) was performed under hydrothermal conditions at 220°C, under autogeneous pressure, with the hydrogel composition calculated starting from the theoretical formula $Na_{0.4}(Al_{1.6}Mg_{0.4}f)Si_4O_{10}(OH,F)_2$. Reactants were mixed in the following order: deionized water, hydrofluoric acid (HF – BDH – 40%), sodium acetate ($NaCOOCH_3$ – Fluka – 99%), magnesium acetate ($Mg(COOCH_3)_2$, 4 H_2O – Fluka – 99%), boehmite (Al_2O_3 – Pural SB1 – Condea – 75 to 78%) and silica (SiO_2 – Aerosil 130 – Degussa – 99.5%). The hydrogel was matured during 2 hours at room temperature (RT) and the pH was measured (pH = 5.5), before being hydrothermally treated in a PTFE lined stainless steel autoclave at 493 K for 72 hours under autogeneous water pressure. After crystallisation, the autoclave was cooled to room temperature. The pH of the supernatant equalled 4.5. The product was then separated by filtration, washed thoroughly with distilled water and dried at 333 K for 12 hours.

The XRD pattern of the sample (Figure 4-13) exhibit the typical hkl bands of Na-montmorillonite, i.e. bands at 15.0 Å (001), 4.45 Å (020, 110), 3,11 Å (004), 2.53 Å (130, 200), 1.68 Å (210) and 1.49Å (060,330).

The results of elemental analyses and TGA listed in Table 4-5 show that there is good agreement with the theoretical composition.

The occurrence of Al for Si substitution in the tetrahedral sheet was proven by ^{27}Al and ^{29}Si MAS NMR. ^{19}F MAS NMR enabled demonstrating of the substitution of Mg for Al in the octahedral sheet.

Table 4-5. Half a unit cell formula calculated from chemical analysis and TGA.

Elemental analyses (weight %)							Half a unit cell formula
Na_2O	MgO	ZnO	Al_2O_3	SiO_2	F	H_2O	
2.34	3.40	–	19.02	55.00	0.20	19.95	$Na_{0.34}[Al_{1.64}Mg_{0.37}f_{0.99}][Si_{4.00}]O_{10}(OH_{1.95}F_{0.05})$, 4.0 H_2O

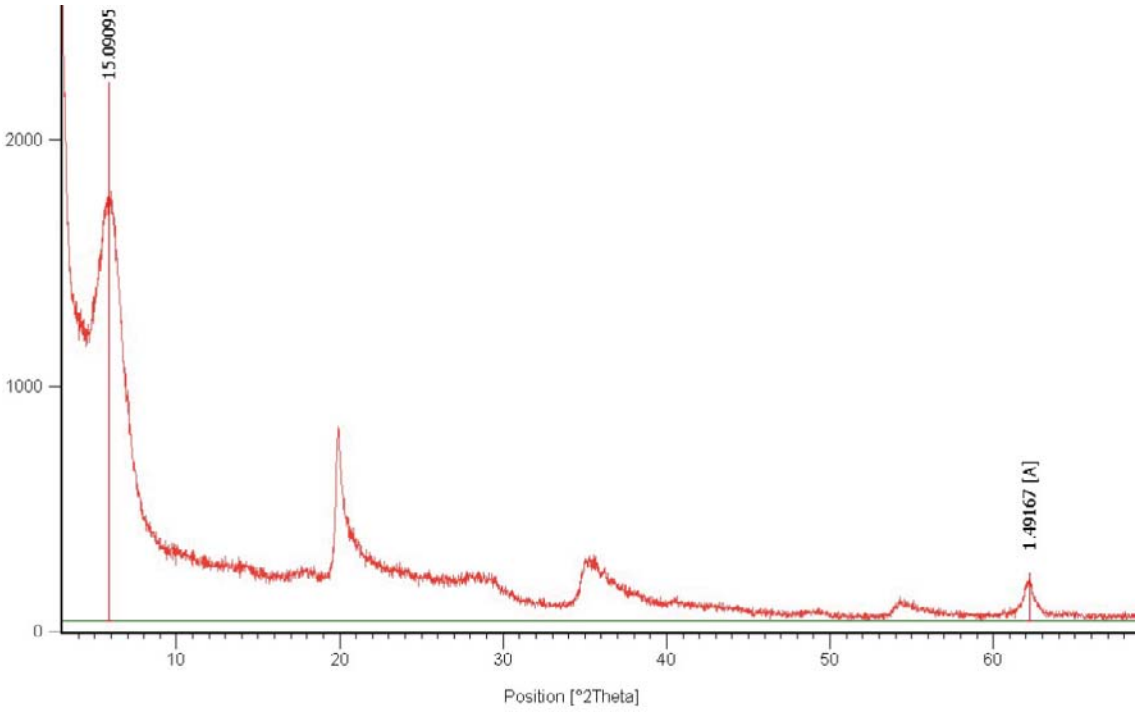

Figure 4-13. *XRD pattern of synthetic Na-montmorillonite*

4.4.2 Experimental procedure

Sample preparations were done inside an acrylic glovebox flushed with N_2. Due to technical problems with the oxygen electrode the O_2 levels could not be measured.

2 g of synthetic Ti-free montmorillonite clay (SMC) was weighted and dispersed in a 0.01 M NaCl salt solution. The suspension was bubbled with N_2 for 30 minutes. The pH in the suspension was measured and left as it was (bulk), or adjusted to pH 2, pH 7.5 or pH 12 with addition of 1 M HCl or 1 M NaOH.

Approximately 2 g of Ti nanopowder (99% purity, SSA 12 m^2/g, American Elements Ltd.) were put inside a dialysis bag (D) (Spectrapore 7, 3,500 MWCO), and added to the suspension. Alternatively, 2 g of Ti powder without dialysis bag or 2 g of Ti foil (99.5 purity, 0.1 mm thick) were added to the suspension. The Ti foil was etched in 1 M HCl overnight and flushed with ethanol before adding it to the suspension. In addition, blank samples without addition of titanium were prepared.

After addition of titanium or empty dialysis bags, the suspensions were purged with nitrogen for another 30 minutes. After purging, sample vessels were closed quickly, the stoppers were tightened with Teflon tape, and the sample vessels were wrapped in aluminium foil to exclude the effect of light, and placed in a heater at 80 °C. The heating setup is presented in Figure 4-14 and all prepared samples are listed in Table 4-6.

Table 4-6. Experimental settings for Ti-bentonite batch tests started on October and November 2009.

Sample number	Label	Ti present	Dialysis bag	T	pH adjustment	Dismantling date
17.	TiNP-SMC-D-80-bulk	2 g, powder	yes	80°C	none	2.3.2010
18.	TiNP-SMC-D-80-bulk2	2 g, powder	yes	80°C	none	ongoing
19.	TiNP-SMC-D-80-pH2	2 g, powder	yes	80°C	2.00	2.3.2010
20.	TiNP-SMC-D-80-pH12	2 g, powder	yes	80°C	12.00	2.3.2010
21.	TiNP-SMC-80-bulk	2 g, powder	no	80°C	none	2.3.2010
22.	TiNP-SMC-80-bulk2	2 g, powder	no	80°C	none	ongoing
23.	TiFO-SMC-80-bulk	2 g, foil	no	80°C	none	2.3.2010
24.	SMC-D-80-bulk	–	yes	80°C	none	2.3.2010
25.	SMC-D-80-pH2	–	yes	80°C	2.00	ongoing
26.	SMC-D-80-pH12	–	yes	80°C	12.00	ongoing
27.	TiNP-D-80-bulk	2 g, powder	yes	80°C	none	ongoing
28.	TiNP-SMC-D-80-pH7,5	2 g, powder	yes	80°C	7.5	ongoing
29.	TiNP-SMC-D-25-bulk	2 g, powder	yes	25°C	none	ongoing
30.	TiNP-SMC-D-25-bulk2	2 g, powder	yes	25°C	none	ongoing

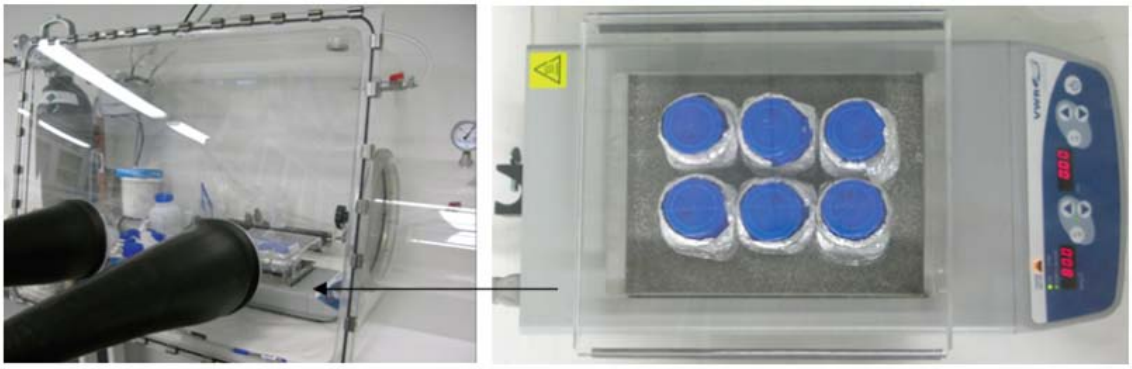

Figure 4-14. *The glovebox and the heating setup.*

After 4.5 months, 6 samples were dismantled by taking out the titanium foil or dialysis bag with Ti nanopowder inside. Thereafter, the clay suspensions were centrifuged for 15 min at 4 000 rpm and the solution was separated from the sedimented clay. The sedimented fraction was washed with pure ethanol, and wet clay samples were sent to PSI for further analysis. The dismantled samples before centrifugation are presented in Figure 4-15.

Solution pH and electric conductivity (EC) were measured inside the glovebox at the end of the experiment. Solutions were filtered through a 0.2 µm pore size membrane filter and analysed for Fe, Na and Ti with ICP-AES at Labtium Oy.

In addition, sample 2 from the first batch series was dismantled after a reaction time of 16.5 months. It was treated similarly but in the open laboratory and it required much longer time to centrifuge after dismantling (~3 h, 4,000 rpm). Subsequently, it was filtered through a 0.45 µm filter before ICP-AES analysis.

4.4.3 Wet chemistry results of samples dismantled at 2.3.2010

The pH of final solutions of all samples was increased (Table 4-7), except for sample 20. Titanium concentrations in solution were below detection limit (0.02 mg/L) in all samples except in sample 2.

Table 4-7. pH, EC and wet chemistry results for the samples dismantled at 2.3.2010.

Sample number	Label	Initial pH	Final pH	EC (µS/cm)	Filter pore size	ICP-AES Fe (mg/l)	Na (mg/l)	Ti (mg/l)
17.	TiNP-SMC-D-80-bulk	5.13	7.01	1,366	0.2 µm	0.03	244	<0.02
19.	TiNP-SMC-D-80-pH2	2.00	4.73	2,520	0.2 µm	<0.03	289	<0.02
20.	TiNP-SMC-D-80-pH12	12.01	10.34	2,320	0.2 µm	<0.03	643	<0.02
21.	TiNP-SMC-80-bulk	5.32	6.86	1,414	0.2 µm	<0.03	272	<0.02
23.	TiFO-SMC-80-bulk	5.19	7.33	1,306	0.2 µm	<0.03	240	<0.02
24.	SMC-D-80-bulk	5.13	7.24	1,327	0.2 µm	<0.03	234	<0.02
2.	TiNP-C-D-bulk2	nd	7.03	1,395	1.2 µm	231	416	5.38
2.	TiNP-C-D-bulk2	nd	7.03	1,395	0.45 µm	174	798	3.67

Abbreviations: nd = not determined

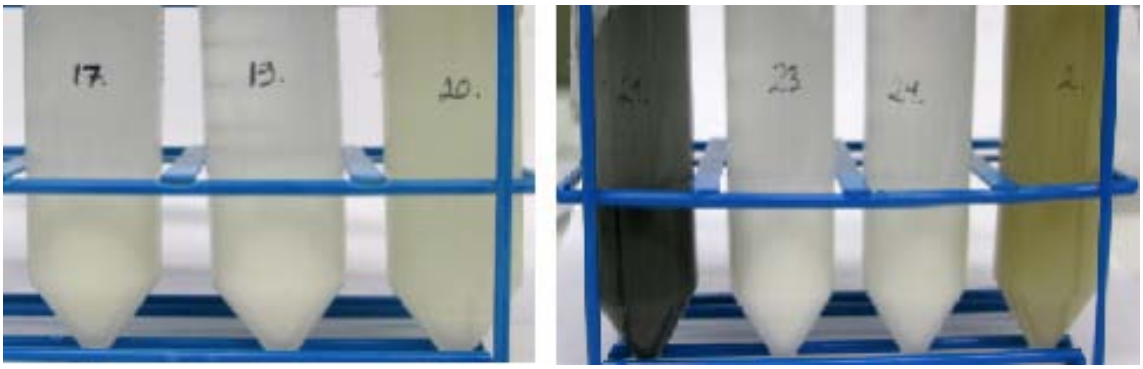

Figure 4-15. *The dismantled (2.3.2010) samples before centrifugation.*

4.5 Spectroscopic data from second experimental series

As described above, the second experimental series were focused on the Ti-clay interaction employing synthetic, *Ti-free* montmorillonite clay (SMC). Concerning the samples produced within this second series of batch tests, the main purpose of the spectroscopic investigations was to establish the Ti concentration prior and after exposure to Ti released by corrosion. Analogous to the first series, the Ti content of different clay samples was analysed by synchrotron-based X-Ray Fluorescence (XRF). These semi-quantitative XRF investigations were conducted at the microXAS Beamline (X05LA) of the Swiss Light Source (for further analytical details see Section 4.3.1). The photon beam intensity and the monochromatic excitation provided by synchrotron X-ray radiation is absolutely needed in order to be able to analyse the present, low-mass, low content samples.

Initially, an identical analytical procedure as compared to the first series was employed. Over the course of the investigations, however, two main differences requested adaptations of the analytical strategy. First, using the synthetic, *Ti-free* montmorillonite clay (SMC), extremely low Ti concentrations are observed. These low Ti contents are due to the indeed low Ti background of the pristine clay material, but are also a result of the moderate Ti transfer rates occurring within the course of the corrosion exposure (despite the efforts to accelerate Ti corrosion). The extremely low concentration of Ti required labour-intensive precautionary measures and quality control procedures to ensure lowest achievable analytical background levels. Second, during the analysis of the different samples, irregularities in the analytical results were noted. These irregularities could be traced down to origin from the presence of metallic Ti contaminations in the samples received. As a consequence, a micro-focused X-ray beam had to be employed in order to obtain reliable analytical results. Using the microbeam allows to localize the contamination hotspots and to identify sample regions free of contamination. These X-ray microbeam measurements were performed using the X-ray microprobe setup available at the microXAS beamline. Aside these two adaptations mentioned, the analytical protocol was identical to the measurements of the first series (see Section 4.3.1).

4.5.1 XRF Results

The first obvious – and important – result is the extremely low Ti content in the samples of the second batch series. Due to this low Ti concentration levels, it was mandatory to investigate the background 'contamination' of the experimental setup at microXAS. After several optimizations steps (mainly improving the collimation of the detector view and replacing the Al sample holder by a PEEK one), no significant Ti signal originating from scattering off of the setup was observed anymore (Figure 4-16, red and yellow lines).

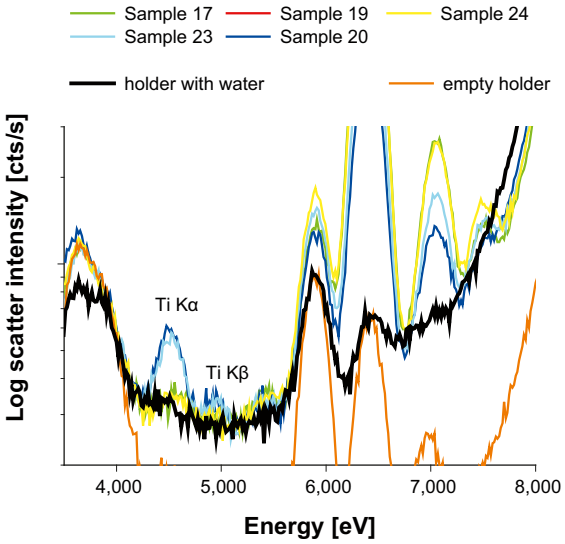

Figure 4-16. *Synchrotron-based XRF spectra showing the Ti content of different synthetic clay samples after exposure to Ti. For samples 20 and 23 the K_α and K_β emission lines of Ti are clearly visible. The other samples exhibit Ti contents at the limit of detection (less than two-fold the background count rate) and are statistically indistinguishable from blank samples.*

Figure 4-16 depicts the initial XRF spectral results obtained using a large X-ray beam with excitation energy 8.5 keV. Only sample 20 and sample 23 show Ti contents significantly above the scattering background of a pure water sample. However, a considerable spatial variability was observed. By changing the X-ray beam imprint position by a few hundreds of micrometers only, the measured Ti fluorescence count rate as indicator for the Ti content was dropping to background levels. This observation stands in inexplicable contrast to the expected chemical homogeneity of wet clay pastes (considering the length-scale of several hundreds of micrometers). The observed spatial variability was further traced down using a micro-focused X-ray beam. For several samples the phenomenon of 'appearance-disappearance' of Ti fluorescence depending on illumination location on the sample was observed. A spatially resolved measurement based on micro-beam application is shown in Figure 4-17 (excitation energy was set to 5.2 keV to enhance Ti signal). A long-distance line scan over the sample holder including the 5mm cavity containing the wet clay paste (sample 19) is depicted. Based on the transmission signal, the 5mm hole in the sample holder plate filled with clay can easily be localized. As predicted, the wet clay paste has an increased absorption as compared to the polycarbonate sample holder frame. In contrast, the Ti fluorescence signal yields an unexpected pattern. One intensive spike corresponding to a Ti 'hot spot' is observed. Based on the intensity of the Ti fluorescence signal and the distinct localization, the presence of a limited number of small Ti particles is proposed (only

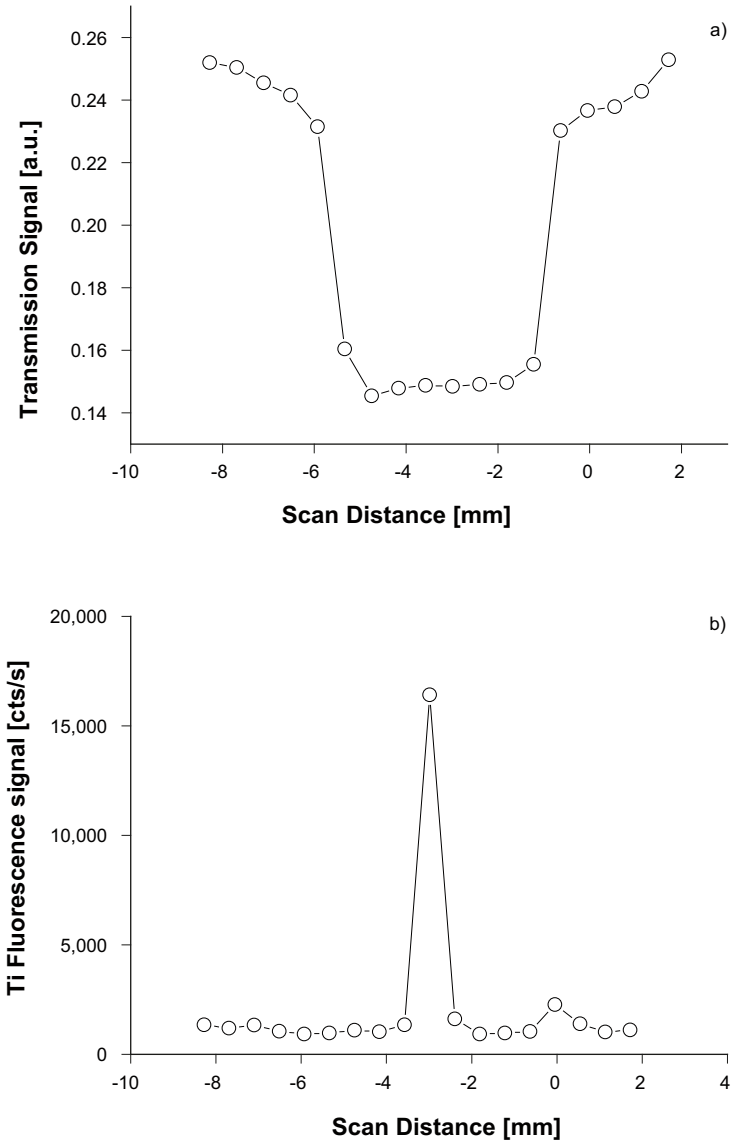

Figure 4-17. *Spatial variability of transmission and Ti K_α fluorescence during a long-distance scan over the sample holder and sample 19. a) Transmission signal indicates location of wet clay paste. b) Ti K_α fluorescence shows a pronounced hot spot, but no enhanced, average Ti content in sample 19.*

one was hit by the depicted line scan). This hypothesis is further supported by XAS spectroscopic measurements (see below). It is important to note, that aside of this one Ti particle, there is no Ti fluorescence signal above background detected over the entire sample. In other words, with the exemption of the 'contamination' by Ti particles, sample 19 is basically free of Ti.

Figure 4-18 shows two long-distance lines scans of sample 23. The two lines scans were measured with a spatial offset (parallel line scans). As for the previous sample, the transmission signal can be used to localize the 5mm hole in the sample holder plate filled with the clay material. Inspecting the corresponding Ti fluorescence, two interesting features become readily apparent. First, in one of the two line scans, the micro-beam is hitting a Ti particle (spike in red scan). Second, for both line scans an elevated, homogenous Ti content is observed. The increase in the Ti fluorescence signal response and the increase in absorption caused by the clay paste coincident in a convincing manner. Consequently, for sample 23 (and only for sample 23) one observes an elevated and constant Ti content dispersed over the entire clay sample material. Such a homogeneous elevated Ti content would

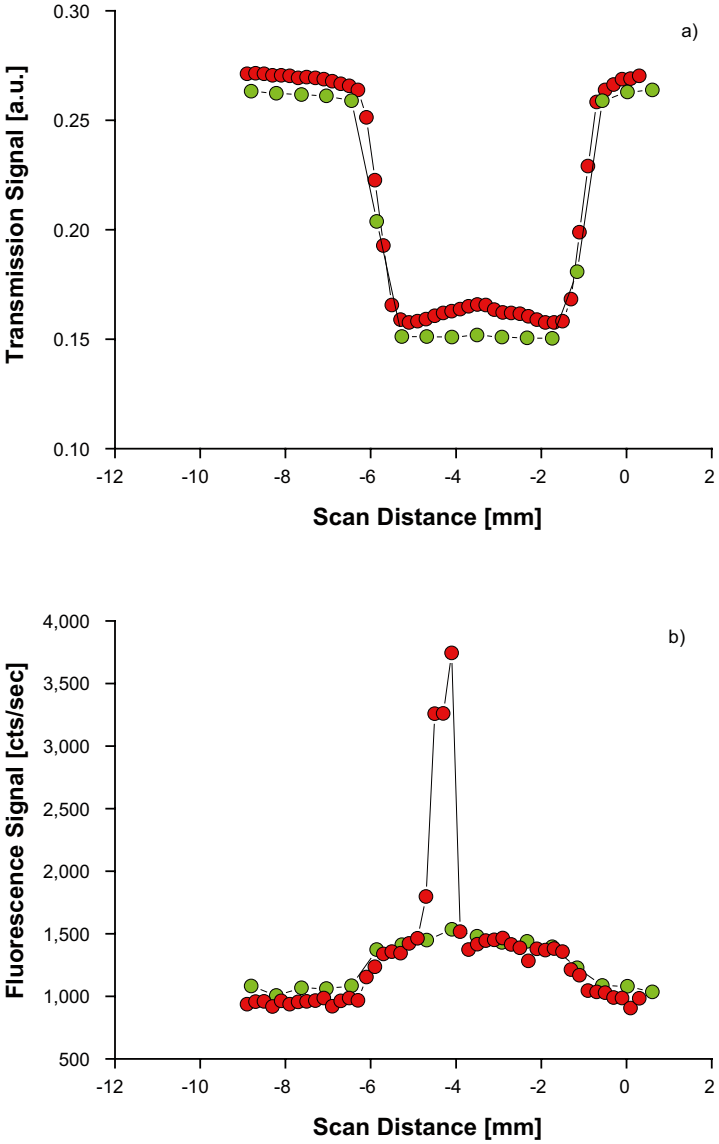

Figure 4-18. *Spatial variability of transmission and Ti K_α fluorescence during two repeated long-distance scans over the sample holder and sample 23 (spatial offset of scans was 500µm). a) Transmission signal indicates location of wet clay paste. b) Ti K_α fluorescence shows an enhanced, average Ti content in sample 23. In one scan a single hot spot is found.*

be expected for geochemical reactions such as (i) Ti incorporated in the octahedral or tetrahedral clay structure, (ii) nano-scale surface precipitation, (iii) Ti pillared clay, etc. However, an X-ray microbeam has to be employed to localize the disturbing contamination hotspots and to identify sample regions free of contamination.

On the phenomena of contamination, hot spots and elevated homogeneous Ti concentrations are further elaborated in Figure 4-19. This figure depicts the XRF spectral results obtained using a micro-focused X-ray beam with excitation energy 5.2 keV. All samples – except one – show a detectable, but weak Ti signal. These samples show a Ti K_{α} fluorescence count rate as low as ~10 cts/sec on top of a ten-fold larger spectroscopic background (scatter and Ca K_{β}, 100cts/sec). All these spectra are identical to the pristine clay material without Ti exposure (sample 24). Only sample 23 yields a significantly larger count rate. At multiple illumination spots on sample 23 nearly identical signals of about 200cts/sec are observed. Highest count rates up to 1,000cts/sec are measured by directing the micro-focused beam onto the localized contamination hot spots.

4.5.2 Preliminary XAS Spectroscopy Results

As detailed above, X-ray Absorption Spectroscopy (XAS) is capable of providing molecular level information regarding the predominant chemical form ('speciation', coordination') of a chosen chemical element. One special XAS-technique, XANES probes the local electronic and coordinative structure of molecular clusters. The corresponding complex features at the elemental absorption edges are frequently used as 'fingerprints' of the prevalent chemical speciation. In the context of the second batch series, preliminary microXANES studies were conducted to enlighten the chemical nature of the observed, localized Ti contaminations. Additional spectroscopic feasibility tests were performed on contamination free regions of sample 23, the only sample for which a measurable Ti transfer was established.

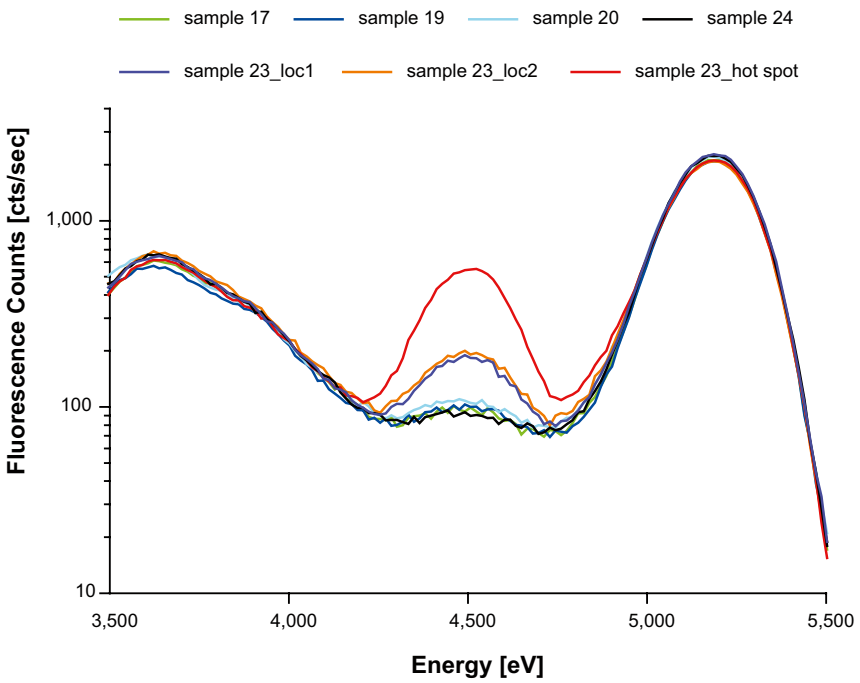

Figure 4-19. *Synchrotron-based micro-XRF spectra showing the Ti content of different synthetic clay samples after exposure to Ti. Only for sample 20 the K_{α} emission line of Ti indicates an elevated Ti content within the entire sample (identical results for different locations). Highest Ti concentration is found at the contamination hot spots.*

Figure 4-20 a) shows the microXANES spectrum obtained for a Ti contamination hot spot. The features at the Ti absorption edge are indicative of a metallic nature of the contamination. The metallic form and the small size point towards a possible cross-contamination with Ti nanopowder, which may have occurred during sample preparation in the glovebox (see Section 4.4.2) as dust from the Ti powder may have contaminated the foil samples that were prepared after the powder samples.

Figure 4-20 b) depicts the microXANES spectrum recorded on the dispersed background ('true Ti on clay'). The Ti found dispersed in the SC shows a non-metallic coordination environment, but also not Ti-oxide. The presence of only one dominant pre-edge transition is indicative of a Ti speciation similar to the Ti coordination environment found in $CaTiSiO_5$ (titanite). The application of advanced data analysis concepts as well as detailed theoretical simulations would be required to elucidate this point in more detail. Nevertheless, the microXANES spectrum shown in Figure 4-20 b) underlines the feasibility of chemical speciation studies within the Ti-SMC system.

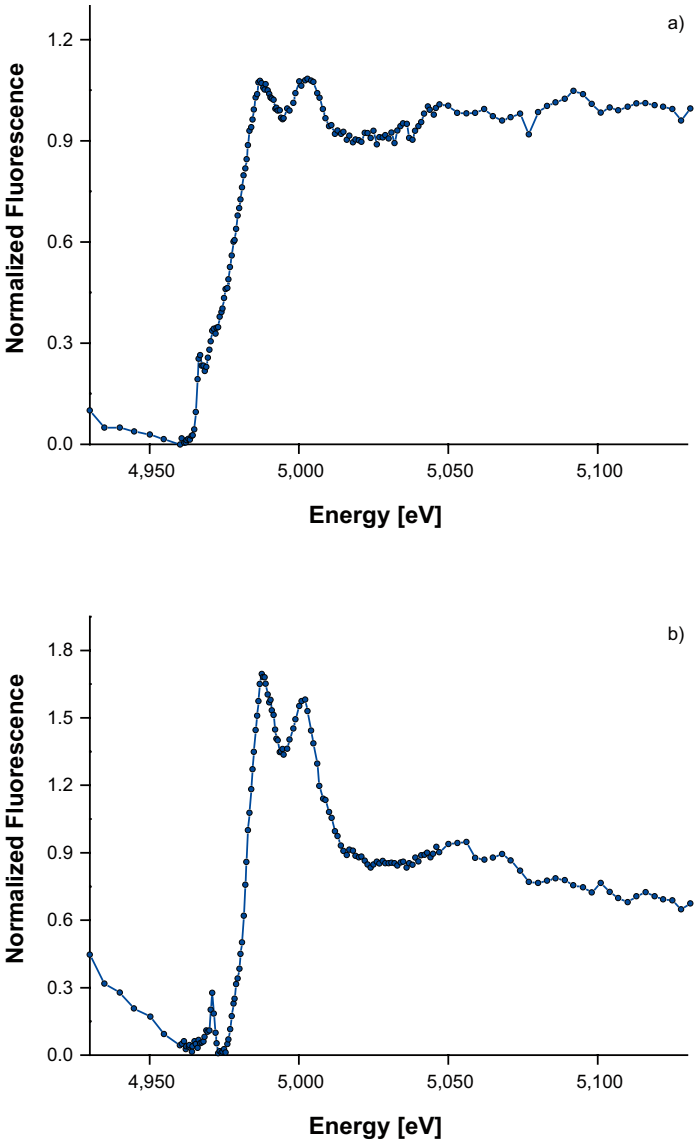

Figure 4-20. *MicroXANES spectra recorded for sample 23. a) microXANES of a localized contamination hot spot. Spectrum is indicative of metallic Ti. b) microXAS of the homogeneous Ti content induced by the corrosion exposure. Characteristic single pre-edge feature points towards a Ti speciation similar to the Ti coordination environment found in $CaTiSiO_5$ (titanite). Note: presented spectra represent preliminary data sets are, e.g. not I0 normalized.*

4.5.3 Preliminary conclusions from second experimental series

Low Ti background concentration in SMC: One of the most important results of the spectroscopic investigations of the second experimental series is the experimental confirmation of the low level Ti background concentration of the new synthetic montmorillonite clay (SMC) material. The availability of Ti-free clay materials represents the most crucial prerequisite for compelling Ti-clay interaction studies.

Ti transfer rates: Only for one sample a significant transfer of Ti could be established: The system having the clay in direct contact with a bulk Ti metal piece. At a first glance, this observation is clearly counterintuitive. Compared to the Ti nanopowder trapped in dialysis bags, the bulk Ti metal piece exhibits a negligible reactive surface area. Consequently, the observed Ti transfer rates should be reduced by orders of magnitude and not – as observed – enhanced. It seems most important to properly address this ambiguity prior to subsequent batch series. For example, it should be clarified if the employed dialysis bags represent a diffusion barrier regarding Ti (possibly strong chemical interaction of aqueous Ti with functional groups of the bag polymers). An alternative rationalization could be related to abrasive processes occurring in the foil-clay suspension (however, preliminary XAS results indicate a Ti molecular environment different from Ti metallic and Ti-Oxide).

Ti contamination: The observed contamination of several samples with small metallic Ti-particles represents a major concern related to the second experimental series. Abundance, spatial characteristics as well as spectroscopic signature point towards the contamination being related to the presence of small Ti particles (use of Ti nanopowder in this experiment series).

In summary, the new SMC represents a very promising clay material to study the interaction of Ti with clay – even down to the level of chemical speciation. However, the experimental conditions influencing the Ti transfer fluxes have to be properly understood (e.g. permeability of dialysis bags regarding Ti) and should optimized (e.g. temperature, and continuous re-adjusting of pH). In particular, the use of Ti nanopowder does not appear to be suitable because of difficult separation of this material from the clay fraction.

5 Summary and Conclusions

Titanium is one of the most immobile elements on the earth's surface. This is a good premise for the use of Ti alloys as supercontainer shell material. It suggests that the performance of the buffer will not be affected and, in addition, that low H_2 gas production will occur. Hence, the effects of Ti-clay interaction on the buffer's safety functions are expected to be insignificant. This statement however needs to be demonstrated with a meaningful programme.

After a feasibility evaluation an experimental pre-study has been started to get insight on the Ti-clay interaction processes. The central part of this study lies in the characterisation of Ti-species in the clay with use of sophisticated spectroscopic methods. The main method used so far is X-ray spectroscopy (XAS) combined with XRF to quantify and characterise Ti-species in the clay samples.

The results obtained so far can be summarized as:

- Natural clay materials contain significant but variable amounts of Ti. The standard purification procedure for bentonites to remove accessories does not or only barely remove Ti.
- The Ti in the most studied clays, such Rokle bentonite, Opalinus Clay, Illite du Puy occurs as microcrystalline TiO_2 (presumably as anatase). On the other hand, the Ti spectra in MX-80 indicate the presence of structural Ti in the clay, but the evidence is not conclusive so far.
- First test series: The exposure of purified MX-80 to titanium powder at room temperature within a period of five months did not lead to measurable additional Ti in the clay. This was even true for samples to acidic or alkaline conditions where corrosion rates and solubility of Ti should be higher.
- Second test series: The use of synthetic montmorillonite combined with the increase of temperature allowed to partly overcome the experimental problems noted in the first series. Thus, Ti background concentrations were effectively very low and Ti transfer to the clay could be identified with spectroscopic analysis for the foil sample. On the other hand, the spectroscopic data highlighted further weaknesses in the setup with Ti nanopowder emplaced in dialysis bags. The results strongly suggest that dialysis bags hinder transfer to the clay. Moreover, the experimental procedure leads to contamination of the clay by nanopowder and thus may mask transfer processes in the analysis.

From these results, preliminary conclusions can be drawn:

- The Ti content in natural bentonites is concentrated mainly in the so-called clay fraction. Ti occurs therein as separate small TiO_2 particles (Rokle) or is incorporated in the structure (MX-80). The properties of natural bentonites are <u>not</u> affected by the Ti originally present in the bentonite clay minerals and/or Ti-oxides. Thus, even at elevated concentrations of Ti (~5% TiO_2) in Rokle, bulk properties (swelling pressure, hydraulic conductivity) are not affected (Karnland et al. 2006).
- The transfer rates of Ti from the metallic source, even in reactive powder form, to the clay are very low and no enrichment above background concentrations after several months could be observed. In order to obtain measurable effects, both the corrosion process must be increased and the background concentration must be reduced.
- The use of synthetic "Ti-free" montmorillonite is a suitable material to carry out Ti-clay interaction experiments and to interpret these in terms of Ti speciation on the clay.
- The use of Ti nanopowder is not recommendable because of difficult separation of this material from the clay which is indispensable for spectroscopic analysis. The use of dialysis bags was not successful in this regard.

Further work

The suggested next step of the experimental Ti-clay interaction study is to carry out a third series of tests with coarser grained Ti and synthetic montmorillonite at temperatures of 80°C and perhaps even higher. The scope thereof is to accelerate processes relevant for repository conditions by increasing Ti transfer rates to the clay. This is a prerequisite for improved spectroscopic analysis of the Ti sorbed and/or precipitated on the clay.

After a period of about half a year, new and old reacted samples will be analyzed and characterized by an adapted spectroscopic procedure.

The results of these data will provide the basis for the continuation and specification of the Ti-clay interaction programme.

References

SKB's (Svensk Kärnbränslehantering AB) publications can be found at www.skb.se/publications.

Azumi K, Seo M, 2003. Corrosion behaviour of titanium-clad carbon steel in weakly alkaline solutions. Corrosion Science, 45, pp 413–426.

Azumi K, Yasiu N, Seo M, 2000. Change in properties of anodic oxide films formed on titanium during long-term immersion in deaerated neutral solutions. Corrosion Science, 42, pp 885–896.

Cornu S, Lucas Y, Lebon E, Ambrosi J P, Luizão F, Rouiller J, Bonnay M, Neal C, 1999. Evidence of titanium mobility in soils profiles, Manaus, central Amazonia. Geoderma, 91, pp 281–295.

Eggleton R A, Foudoulis C, Varkevisser D, 1987. Weathering of basalt: changes in rock chemistry and mineralogy. Clays and Clay Minerals, 35, pp 161–169.

Fitzpatrick R W, le Roux J, Schwertmann U, 1978. Amorphous and crystalline titanium and iron-titanium oxides in synthetic preparations, at near ambient conditions, and in soil clays. Clays and Clay Minerals, 26, pp 189–201.

Hua F, Mon K, Pasupathi P, Gordon G, Shoesmith D W, 2004. Corrosion of Ti grade 7 and other Ti alloys in nuclear waste repository environments – a review. Corrosion/2004, NACE International, Houston, Texas, Paper 04689.

Jalava J-P, Hiltunen E, Kähkönen H, Erkkilä H, Härmä H, Taavitsainen V-M, 2000. Structural investigation of hydrous titanium dioxide precipitates and their formation by small-angle X-ray scattering. Industrial & Engineering Chemistry Research, 39, pp 349–361.

Jepson W B, 1988. Structural iron in kaolinites and in associated ancillary minerals. In: Stucki J P, Goodman B A, Schwertmann U (eds). Iron in soils and clay minerals. Dordrecht: Reidel, pp 467–536.

Johnson L, Marschall P, Wersin P, Gribi P, 2005. HMCBG processes related to the steel components in the KBS-3H disposal concept. Posiva Working Report 2005-09, Posiva Oy, Finland.

Karnland O, Olsson S, Nilsson U, 2006. Mineralogy and sealing properties of various bentonites and smectite-rich clay materials. SKB TR-06-30, Svensk Kärnbränslehantering AB.

King F, 2007. A review of the properties of alternative materials for the KBS-3H supercontainer and their impact on long-term safety. Draft report. /är den publicerad?; referenslistan får inte innehålla opublicerat material/

Maeds R E, Malden P J, 1975. Electron spin resonance in natural kaolinites containing Fe (super 3+) and other transition metal ions. Clay Minerals, 10, pp 313–345.

Malengreau N, Muller J-P, Calas G, 1995. Spectroscopic approach for investigating the status and mobility of Ti in kaolinitic materials. Clays and Clay Minerals, 43, pp 615–621.

Mattsson H, Olefjord I, 1984. General corrosion of Ti in hot water and water saturated bentonite clay. SKB/KBS TR 84-19, Svensk Kärnbränslehantering AB.

Mattsson H, Olefjord I, 1990. Analysis of oxide formed on Ti during exposure in bentonite clay. I. The oxide growth. Materials and Corrosion, 41, pp 383–390.

Mattsson H, Changai L, Olefjord I, 1990. Analysis of oxide formed on Ti during exposure in bentonite clay. II. The structure of the oxide. Materials and Corrosion, 41, pp 578–584.

Meunier A, 2005. Clays. Berlin: Springer.

Morad S, Aldahan A A, 1982. Authigenesis of titanium minerals in two proterozoic sedimentary rocks from Southern and Central Sweden. Journal of Sedimentary Petrology, 52, pp 1295–1305.

Nesbitt H W, 1979. Mobility and fractionation of rare earth elements during weathering of a granodiorite. Nature, 279, pp 206–210.

Puigdomenech I, 2004. Hydra/Medusa: Chemical Equilibrium Database and Plotting Software. Royal Institute of Technology (KTH), Sweden. Available at: http://www.kemi.kth.se/medusa/.

Rengasamy P, 1976. Substitution of iron and titanium in kaolinites. Clays and Clay Minerals, 24, pp 265–266.

Romero A, Dorado F, Asencio I, García P B, Valverde J L, 2006. Ti-pillared clays: synthesis and general characterization. Clays and Clay Minerals, 54, pp 737–747.

Roy P S, 1999. Heavy mineral beach placers in southeastern Australia: their nature and genesis. Economic Geology, 94, pp 567–588.

Schroeder P A, Shiflet J, 2000. Ti-bearing phases in the Huber formation, an East Georgia kaolin deposit. Clays and Clay Minerals, 48, pp 151–158.

Schutz R W, 2005. Corrosion of titanium and titanium alloys. In: Cramer S D, Covino B S Jr (eds). ASM Handbook. Vol. 13B, Corrosion: materials. Materials Park, OH: ASM International, pp 252–299.

SKB, 2008. Horizontal deposition of canisters for spent nuclear fuel. Summary of the KBS-3H project 2004–2007. SKB TR-08-03, Svensk Kärnbränslehantering AB. (Also published as Posiva 2008-03, Posiva Oy, Finland.)

Sterte J, 1986. Synthesis and properties of titanium oxide cross-linked montmorillonite. Clays and Clay Minerals, 34, pp 658–664.

Tilley D B, Eggleton R A, 2005. Titanite low-temperature alteration and Ti mobility. Clays and Clay Minerals, 53, pp 100–107.

Vogt K, Köster H M, 1978. Zur Mineralogie, Kristallchemie und Geochemie einiger Montmorillonite aus Bentoniten. Clay Minerals, 13, pp 25–43.

Weaver C E, 1976. The nature of TiO2 in kaolinite. Clays and Clay Minerals, 24, pp 215–218.

Wersin P, Birgersson M, Olsson S, Karnland O, Snellman M, 2008. Impact of corrosion-derived iron on the bentonite buffer within the KBS-3H disposal concept – the Olkiluoto site as case study. Posiva 2007-11, Posiva Oy, Finland.

XRF analyses

Element	Description Method	OPA MT 4.01 / 0.0 / 0.97 Geo-2370	MX-80 raw 4.04 / 0.0 / 0.89 Geo-2370	MX-80 pur. 1.03 / 3.17 / 0.92 Geo-2370	Rokle 4.01 / 0.0 / 0.91 Geo-2370
Na	%	0.266	0.28	< 0.14	< 0.19
Na	Abs. Error (%)	0.074	0.053	–0.079	0
Mg	%	1.026	0.509	0.293	0.647
Mg	Abs. Error (%)	0.024	0.014	0.014	0.024
Al	%	7.447	3.834	0.9551	4.152
Al	Abs. Error (%)	0.022	0.013	0.0098	0.02
Si	%	16.32	13.89	36.38	14.06
Si	Abs. Error (%)	0.03	0.02	0.05	0.03
P	%	0.0567	0.01705	< 0.0010	0.2012
P	Abs. Error (%)	0.0012	0.00048	0	0.0016
S	ppm	2,632	1,253	< 20	131
S	Abs. Error (ppm)	11	6	0	2.3
Cl	ppm	278.1	27.2	< 1.5	< 3.1
Cl	Abs. Error (ppm)	2.6	0.5	0	0
K	%	2.13	0.2607	0.1482	0.6246
K	Abs. Error (%)	0.005	0.0012	0.0009	0.0026
Ca	%	6.034	0.6688	0.01504	1.676
Ca	Abs. Error (%)	0.008	0.0015	0.00032	0.004
Ti	%	0.4612	0.05492	0.02399	2.324
Ti	Abs. Error (%)	0.0013	0.00034	0.00025	0.003
V	ppm	123.6	11.5	6.3	345.6
V	Abs. Error (ppm)	4.6	1.1	0.9	8.9
Cr	ppm	121.9	15.4	10.2	93.7
Cr	Abs. Error (ppm)	1.4	0.3	0.3	1.3
Mn	%	0.0376	0.00832	0.00273	0.1156
Mn	Abs. Error (%)	0.0002	0.00006	0.00004	0.0003
Fe	%	3.777	2.15	0.4634	10.76
Fe	Abs. Error (%)	0.006	0.004	0.0017	0.01
Co	ppm	30.8	14.4	9.5	52.6
Co	Abs. Error (ppm)	5.5	3.1	2.4	8
Ni	ppm	63.6	4.7	1.1	52.5
Ni	Abs. Error (ppm)	1.9	0.7	0.7	2.3
Cu	ppm	18.8	5.5	6.9	175.4
Cu	Abs. Error (ppm)	0.9	0.4	0.4	2.7
Zn	ppm	91.7	65.6	7.6	174.2
Zn	Abs. Error (ppm)	1.4	1	0.5	2.2
Ga	ppm	22.4	23.9	7.2	23.2
Ga	Abs. Error (ppm)	0.7	0.6	0.3	0.9
Ge	ppm	1.9	< 0.4	0.5	1.5
Ge	Abs. Error (ppm)	0.3	–0.3	0.2	0.4
As	ppm	6.4	7.5	0.4	8.6
As	Abs. Error (ppm)	0.5	0.5	0.3	0.6
Se	ppm	0.7	< 0.3	< 0.2	1
Se	Abs. Error (ppm)	0.2	–0.2	0	0.3
Br	ppm	3.5	0.8	0.3	2.5
Br	Abs. Error (ppm)	0.2	0.2	0.2	0.3
Rb	ppm	120.8	12.4	6.3	46.8
Rb	Abs. Error (ppm)	0.7	0.2	0.2	0.5
Sr	ppm	270.2	239.7	8.2	332.9
Sr	Abs. Error (ppm)	0.9	0.7	0.2	1.2

Element	Description Method	OPA MT 4.01 / 0.0 / 0.97 Geo-2370	MX-80 raw 4.04 / 0.0 / 0.89 Geo-2370	MX-80 pur. 1.03 / 3.17 / 0.92 Geo-2370	Rokle 4.01 / 0.0 / 0.91 Geo-2370
Y	ppm	23.1	39.4	11.3	32.1
Y	Abs. Error (ppm)	0.5	0.4	0.3	0.6
Zr	ppm	131.1	179.1	73.3	435.8
Zr	Abs. Error (ppm)	0.7	0.7	0.4	1.3
Nb	ppm	18.9	24.9	9	122.3
Nb	Abs. Error (ppm)	0.2	0.2	0.2	0.5
Mo	ppm	1.1	6.4	< 0.5	7.1
Mo	Abs. Error (ppm)	0.3	0.5	–0.3	0.8
Ag	ppm	< 0.3	< 0.2	< 0.2	1.9
Ag	Abs. Error (ppm)	0	0	0	0.2
Cd	ppm	< 0.2	< 0.2	< 0.2	1.9
Cd	Abs. Error (ppm)	–0.2	–0.2	0	0.2
In	ppm	< 0.3	< 0.2	< 0.2	< 0.3
In	Abs. Error (ppm)	0	0	0	0
Sn	ppm	4.2	10	2.8	5.9
Sn	Abs. Error (ppm)	0.2	0.2	0.1	0.2
Sb	ppm	< 0.4	1.6	< 0.3	1.5
Sb	Abs. Error (ppm)	0	0.2	0	0.2
Te	ppm	0.3	< 0.3	< 0.3	< 0.4
Te	Abs. Error (ppm)	0.2	0	–0.2	0
I	ppm	< 1.0	< 1.0	< 0.9	< 1.1
I	Abs. Error (ppm)	0	0	0	0
Cs	ppm	2.1	< 1.7	< 1.6	< 1.9
Cs	Abs. Error (ppm)	0.6	0	–0.6	0
Ba	ppm	295.6	377.8	115.4	702.3
Ba	Abs. Error (ppm)	1.9	2	1.6	2.5
La	ppm	32.8	49.4	21.5	86.7
La	Abs. Error (ppm)	2	2.1	1.9	2.2
Ce	ppm	73.6	123.8	43.5	214.1
Ce	Abs. Error (ppm)	2.8	2.9	2.6	3
Pr	ppm	< 7.6	21.1	11.5	23.1
Pr	Abs. Error (ppm)	–5.3	4.5	4.2	4.3
Nd	ppm	31.4	62.2	28.1	95.3
Nd	Abs. Error (ppm)	5.3	5.8	5.2	5.7
Sm	ppm	17.8	20.6	12.1	28.9
Sm	Abs. Error (ppm)	0.6	0.4	0.3	0.7
Hf	ppm	4.8	6.9	2.2	12.4
Hf	Abs. Error (ppm)	1.7	1.2	1.1	4
Ta	ppm	< 5.7	< 3.1	< 3.3	18.5
Ta	Abs. Error (ppm)	–4.6	–1.9	–1.2	7.4
W	ppm	7.5	3.8	< 1.7	5.3
W	Abs. Error (ppm)	1.7	0.8	–0.7	1.9
Hg	ppm	< 1.1	< 0.7	< 0.7	0.8
Hg	Abs. Error (ppm)	0	–0.2	0	0.6
Tl	ppm	0.5	1	< 0.6	1.5
Tl	Abs. Error (ppm)	0.3	0.3	0	0.5
Pb	ppm	19.7	38.5	14	15.5
Pb	Abs. Error (ppm)	0.9	0.9	0.6	1
Bi	ppm	< 1.0	1	< 0.6	< 1.4
Bi	Abs. Error (ppm)	0	0.4	0	0
Th	ppm	11.1	26.8	12.7	13.2
Th	Abs. Error (ppm)	0.5	0.6	0.4	0.7
U	ppm	< 2.1	7.8	2.8	1.3
U	Abs. Error (ppm)	0	0.7	0.5	1.1